VEHICLE DAMAGE PREDICTION AFTER IMPACT

A Dissertation
Presented to
The Academic Faculty

by

Ishit Bhadresh Amin

In Partial Fulfillment
of the Requirements for the Degree
Master of Science in Mechanical Engineering

Georgia Institute of Technology
May 2020

VEHICLE DAMAGE PREDICTION AFTER IMPACT

Approved by:

Dr. Bert Bras, Advisor
School of Mechanical Engineering
Georgia Institute of Technology

Dr. Michael Leamy
School of Mechanical Engineering
Georgia Institute of Technology

Dr. David Torello
School of Mechanical Engineering
Georgia Institute of Technology

Date Approved: December 11, 2019

ACKNOWLEDGEMENTS

I would like to thank Dr. Bert Bras for the opportunity to work on this project and his advice and guidance through my work. I would also like to thank my committee members, Dr. Michael Leamy and Dr. David Torello, for their support and encouragement.

Additionally, I would also like to thank Joe Rork and Larry Coan at the Ford Motor Company, who supported and provided guidance throughout my work. And a big thank you to everyone in the Sustainable Design and Manufacturing lab for their feedback and great conversations.

I would also like to thank my friends and family for their support throughout my time in school, and specifically my parents, who have supported me in everything I do and without whom, I would not have access to the opportunities that I do.

TABLE OF CONTENTS

LIST OF TABLES

LIST OF FIGURES

LIST OF SYMBOLS AND ABBREVIATIONS

ADAS	Advanced Driver-Assistance System
FEM	Finite Element Method
Crush	Intrusion of exterior line
ACC	Adaptive Cruise Control
LPM	Lumped Parameter Model
PDOF	Principle Degree of Force

SUMMARY

As more new vehicles begin to be offered with advanced driver assistance systems (ADAS), can these systems be used to determine which parts are damaged on a car after an accident as occurred? To answer this question, crash modeling techniques were reviewed along with literature regarding ADAS sensors. Although there is no published work showing the use of ADAS sensors for crash damage prediction, this paper uses a combination of current crash modeling techniques and ADAS data to propose and tests a new system for crash damage prediction.

Current crash modeling techniques such as finite element methods (FEM) can provide a detailed analysis of vehicle response. However, FEM tends to be very complicated to setup and requires information that would only be available to vehicle manufacturers. So, to avoid this, lumped parameter models that provide similar results were devised. However, lumped parameter models used for crash modeling require new coefficients for every crash scenario desired. To avoid this, a much simpler approach is utilized in this paper, crash pulse analysis. Crash pulse analysis can be used to calculate crush or the intrusion on the exterior line of the vehicle. The crush value can be combined with impact location to predict which parts are damaged on the vehicle.

The damage prediction method proposed in this paper has three main steps: crush prediction, impact zone prediction, and determining damaged parts. Impact zones are parts of the perimeter of the vehicle that have been divided by ADAS sensor locations and vehicle part locations. To determine the crush value, crash pulse analysis is used and to determine the impact zone, parking sensor and adaptive cruise control radar data is

analyzed. Once crush and impact zone are obtained, they can be used to determine which parts are damaged on the vehicle. In this paper, however, the effect of crush errors and impact zone errors are analyzed when determining damaged parts.

The proposed system is tested using National Highway Traffic Safety Administration (NHTSA) crash test data for crush prediction and simulated ADAS data for impact zone prediction. This paper used 76 different crash tests to determine an average error of -12.1% for crush prediction. There are also errors for impact zone prediction, which are limited by the ADAS sensor specifications and sensor placement. The effect of both errors on the final part of the system is limited. Assessing the errors for a 2016 Ford Fusion Energi, errors for crush values above 18 [cm] did not have a significant effect on the final determination of damaged parts. Additionally, impact zone errors do affect the final determination of damaged parts, however, only if the errors are due to impact scenarios outside the ADAS sensor specifications.

Overall, NHTSA data proved the crush prediction part of the proposed system and the simulated data proved the impact zone prediction part of the proposed system. The errors resulting from both were used to assess the feasibility of determining damaged parts. It can be concluded that crush and impact zone location, even with error, can be used to determine which parts are damaged on the vehicle.

CHAPTER 1. INTRODUCTION

The primary function of current advanced driver assistance systems (ADAS) is to provide drivers with real-time advice, warning, and instructions (Karel A. Brookhuis, 2001). Implementing ADAS systems should decrease traffic accidents that are attributed to human failure, which accounted for about 90% of all traffic accidents as concluded by Smiley and Brookhuis (1987). As these systems are just beginning to be offered as standard equipment on new cars, their effect will become more evident in the coming years. The net result of ADAS implementation would be a decrease in the number of accidents; however, accidents cannot be completely eliminated. This leads to an interesting question, can ADAS systems be used to predict which parts are damaged on a car after an accident has occurred? To answer this question, accident reconstruction and damage prediction methods were researched along with sensors related to different driver assistance systems.

Originally, the goal of this thesis was to make one of three determinations after an impact: if the car is drivable with a light damage, if the car is repairable with extensive damage, or if the car is totaled. This is useful information for section 1.3 and parts of section 4.3 as those sections address the results from the algorithm presented in this paper.

1.1 Crash Modeling Techniques

Modeling and analysis of vehicle crashes originated with automotive manufacturers attempting to reduce the number of expensive crash tests that had to be conducted for new vehicles. Not only does modeling save manufacturers from the potential of conducting expensive crash tests, but it also allows them to begin analyzing crash test capabilities

earlier in the design cycle. Finite element method (FEM) is considered the most thorough tool to gain insight into vehicle crashworthiness (H. R. K. Witold Pawlus, and Kjell G. Robbersmyr, 2013). Although FEM models are accurate, they require powerful computational resources to simulate impacts. Additionally, their accuracy depends on correctly selecting material properties and generating appropriate mesh sizes for the model. It is widely accepted that if results from a FEM model do not correlate with a physical test, then the model is considered wrong (Paul Baguley, 2009).

Due to the complexity and cost associated with FEM models, lumped parameter modeling of viscoelastic systems is frequently used as a secondary approach. There are various types of lumped parameter models, but the models used and referenced most frequently in literature are the Kelvin and Maxwell models. For every lumped parameter model used for crash analysis, the structural parameters of the model like stiffness and damping are estimated based on a given crash scenario (H. R. K. Witold Pawlus, and Kjell G. Robbersmyr, 2013). This results in accurate models; however, the obtained parameters cannot be used to simulate different crash scenarios. For the purposes of this thesis and the system developed, it is important that the system be versatile; therefore, a data-based approach is used for the analysis conducted.

There are numerous data-based models that can be used to predict crash analysis data, a type of time series data. These methods include several nonlinear autoregressive (NAR) models, special cases of which are shown to be feedforward neural networks (Connor JT, 1994). As the previous paragraph states, a lumped parameter model is limited to the crash test scenario used to calculate its stiffness and damping coefficients. A NAR model can be used to overcome this drawback of a lumped parameter model by reproducing

the kinematics of a vehicle under different collision circumstances (H. R. K. Witold Pawlus, and Kjell G. Robbersmyr, 2013). Both the data-based approach and the standard approach to lumped parameter modeling can be used to obtain the dynamic crush or intrusion on the exterior line of the car. Figure 1-1 below shows a visual to explain dynamic crush, which will be referred to as "crush" throughout the rest of this paper.

Obtaining crush is a much simpler when compared to methods used to develop lumped parameter model. Having access to the accelerometer measurements from a real crash means we can perform basic integration on the signal to obtain velocity and displacement (H. R. K. Witold Pawlus, Kjell G. Robbersmyr, 2010). At the time when the relative approach velocity is zero, the maximum dynamic crush occurs. More information on FEM modeling, the Kelvin and Maxwell models, and data-based modeling is provided in chapter 2.

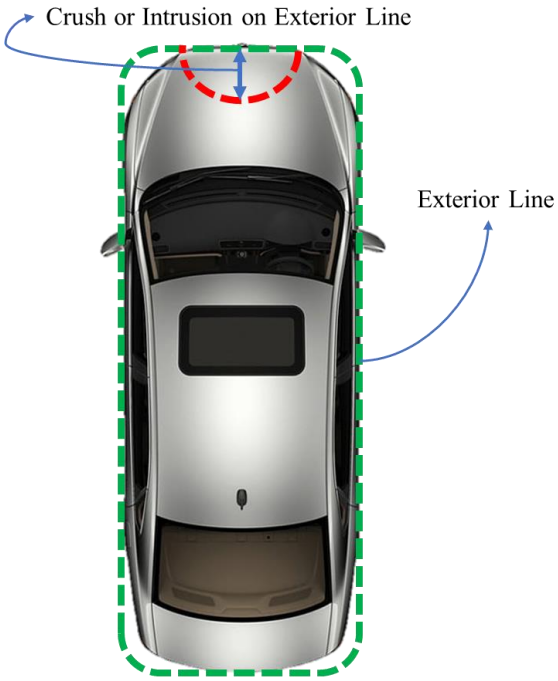

Figure 1-1: Crush Visual

1.2 Introduction to ADAS

From section 1.1, it is evident that there are various methods available for crash analysis and modeling; however, none of the methods covered use ADAS sensor data as inputs. This is due to a lack of literature available in the area of crash damage prediction using ADAS sensors. The rest of section 1.2 provides a brief introduction to the ADAS systems available today.

1.2.1 Overview of modern ADAS

There are several types of ADAS systems fitted to new cars, systems such as lane keeping assist, automatic braking, and adaptive cruise control. Figure 1-2 below provides an overview of how ADAS sensors are used and provides an insight into their placement. Breaking it down, all ADAS systems rely on some combination of vision sensors, light detection and ranging (LIDAR), radar, and ultrasonic sensors (Vipin Kumar Kukkala, 2018). The radar is used for adaptive cruise control (ACC), cross-traffic alert, and rear collision warning. The LIDAR system and radar are used for automatic breaking and pedestrian detection. Camera systems are used for lane keep assist and surround view features such as a backup camera and a surround view camera system. Finally, ultrasonic sensors are used for park-assist features.

For this thesis, lane keep assist, park assist, adaptive cruise control, emergency breaking, and blind-spot detection were considered. Every feature considered uses three

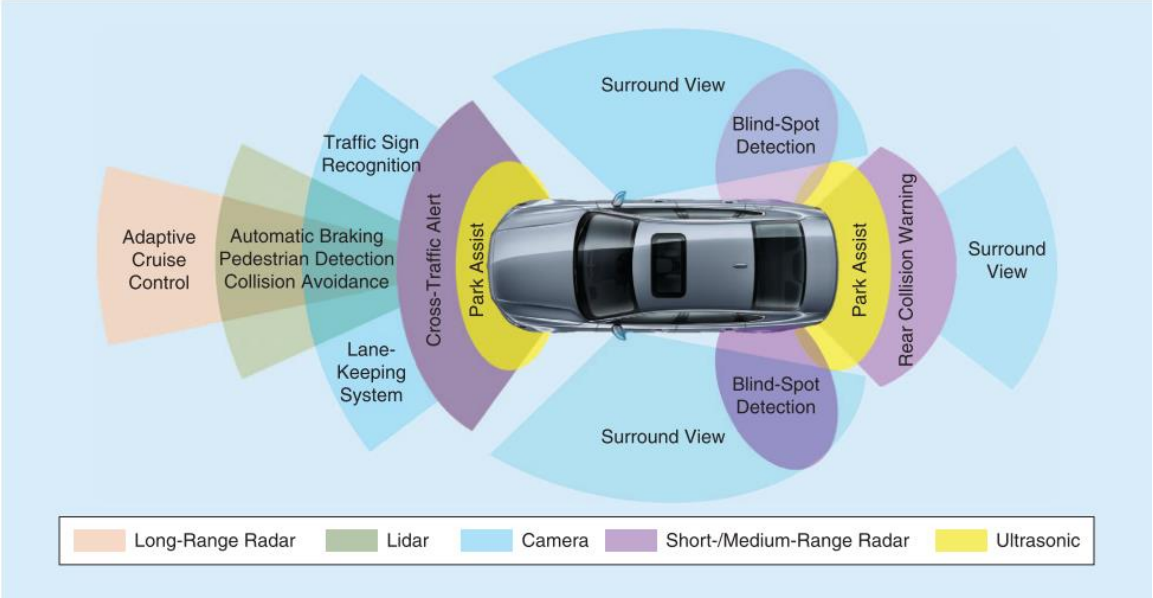

Figure 1-2: Overview of current ADAS sensors (Vipin Kumar Kukkala, 2018)

basic sensors, cameras, ultrasonic sensors, and radar. After assessing the ease of access to data from each sensor, the ultrasonic sensors and radar were the only ADAS sensors used. Chapter 3 provides a more detail on the decision to use two ADAS sensors rather than all that were available.

1.3 Crash damage prediction using traditional crash modeling and ADAS

This paper focuses on crash damage prediction using ADAS data in lieu of more complicated lumped parameter models and FEM simulations. As discussed in section 1.1, if accelerometer data is available, then velocity and displacement can be obtained by integrating the acceleration signal, which gives crush. Having crush provides the same information that could be obtained via lumped parameter models. However, estimating crush by itself is useless as it does not provide an area of the car where the damage occurred. By observation, a crush value for a front impact would cause different parts to be damaged than the same value would for a rear impact.

To obtain the impact location, the ADAS sensors mentioned in earlier can be used. In section 1.2, it was stated that the ADAS sensor used for this thesis were the ultrasonic sensors and radar. As observed from figure 1-2, radar sensors can be placed around the car for various systems. However, many vehicles use radar primarily for ACC, so for this thesis, it is assumed that there is a single radar at the front for ACC. Then combining the sensors available, from figure 1-2, the ultrasonic sensors and the radar cover the front and the rear of the vehicle. So, data from both of those sensors can be used to predict the impact location for a front or rear impact.

Earlier in chapter 1, it is mentioned that the original goal of this work was to make one of three determinations after an impact occurs: if the car is drivable with light damage, if the car is repairable with extensive damage, or if the car is totaled. Due to this initial goal, accuracy errors in crush predication can be forgiven if there is minimal effect on the final result. As the results section will show, this is true for many impact scenarios. To summarize, a combination of crush and location can be obtained using time-series data from the accelerometer, ultrasonic sensors, and radar. Chapter 3 will specify the time limit for data from each sensor.

CHAPTER 2. LITERATURE REVIEW

Chapter 2 provides an overview of the literature and previous work done in the fields of vehicle crash mechanics, accident damage prediction, and potential ADAS uses for accident damage prediction. The research that was conducted for this thesis began with a literature review, thus, this chapter will provide an overview of the actual process used to get to the methods presented in chapter 3.

Chapter 1 presented the main question for this paper, can ADAS systems be used to predict which parts are damaged on a car after an accident has occurred? To answer that question, a search was conducted to find literature and previous work dealing with predicting post-crash damage using ADAS sensors. However, the search did not result in any useful information. Thus, the question had to be split up into two separate problems, the first one was to simply study the current crash analysis methods as done in section 2.1. This would provide a good foundation to introduce ADAS data to. Which leads to the second problem, can ADAS data be used along with a crash analysis method? The requirement for this was that the final solution be more versatile than traditional crash analysis methods and that it require less scenario specific input data.

2.1 Current Accident Reconstruction Methods

As discussed in chapter 1, there are several accident reconstruction methods, with the most prominent one being finite element methods. However, due to their cost and complexity, lumped parameter models are often used in their place. Lumped parameter models also have some drawbacks such as the stiffness and damping coefficients being scenario specific. This can be solved by a data based approach to lumped parameter modeling. And finally, crash pulse analysis can be conducted to directly solve for

displacement, which can be used to solve for crush. Each of the methods mentioned in this paragraph are discussed for the rest of section 2.1.

2.1.1 Finite Element Model

Finite element models (FEM) are widely used for modeling large deformation crash problems in the area of crashworthiness. As computational resources become more economical, FEM analysis of vehicles becomes more complex and sophisticated. This is done with the final goal being that the model output matches physical tests. FEM is considered the most powerful tool in vehicle crash analysis (Muraspahic, 2013), however, due to its complexity, it is more expensive and time consuming to run than the other vehicle crash modeling techniques. There are several types of FEM software packages available, codes such as LS-DYNA, PAM-CRASH, RA-DIOSS, and NASTRAN. LS-DYNA and NASTRAN are most frequently used out of the ones mentioned. Specifics about the previously mentioned FEM codes are not discussed in this thesis as they were not used, but literature on each code is widely available. When discussing FEM for crash analysis, it is important to discuss the cost and complexity associated with it. Generally, FEM costs involve computational cost and the cost of labour, both of which are discussed below.

Breaking down cost estimates for vehicle crash analysis conducted using FEM, it can be seen that labour costs are the main direct cost element involved (Paul Baguley, 2009). Assessing the labour costs, Baguley et al. work shows that meshing has the largest cost contribution followed by validation and interpretation of the results. This goes to show the importance of meshing, which is an integral part of setting up an FEM simulation. The cost associated with meshing and analysing results goes to show how complex finite

element simulations are. Due to the cost and complexity of FEM simulations, lumped parameter modeling is often used in its place. Lumped parameter models are cheaper and much less complex than FEM models, and some models, if set up correctly, have the same results (Huang, 2002).

2.1.2 Lumped Parameter Modeling

Lumped parameter models (LPM) have been research for the purposes of finding a cheaper solution to FEM analysis. LPMs in their simplest form, are used to model mass-spring-damper systems. However, they can be used to model numerous different systems from electrical systems to vibrations in jet engines. Since the focus of this thesis is on vehicle crash modeling, models developed for crash analysis will be discussed. There are various types of LPMs available for crash analysis, and due to their simplicity in comparison with FEM, custom models can be made depending on result requirements. The two main models used in literature are the Kelvin and the Maxwell models. There are other models available, however, for the purposes of this paper, the Kelvin and Maxwell models will be discussed.

The Kelvin model, as shown in figure 2-1 (a), is a mass-spring-damper system with the spring and damper connected in parallel. In a majority of cases, the response from a system like the Kelvin model is underdamped, therefore emphasis is placed on underdamped behaviour (Pawlus, 2011). For a car crash, it is going to have F, an external force and y, the displacement of the mass, as shown in figure 2-1 (b). Using figure 2-1 (b), the equation of motion (EOM) can be written as follows in equation (1):

$$\boldsymbol{u(t) = m\ddot{y} + c\dot{y} + ky} \tag{1}$$

In equation (1), $u(t)$ is the external force changing with time, $\ddot{y}$ is acceleration, and $\dot{y}$ is velocity. There are multiple methods to estimate the parameters of the Kelvin model, they are described below. Continuing with the model itself, the input is the initial impact velocity and to validate it, an input force is needed shown as $u(t)$ in equation (1). From Pawlus et al., it is stated that the force acting on the car during the crash is the acceleration in the opposite direction, multiplied by the mass according to Newton's 2nd law. This is in the equation below:

$$u(t) = -m\ddot{y}$$

Combining this with equation (1), gives the following as equation (2):

$$-m\ddot{y} = m\ddot{y} + c\dot{y} + ky \tag{2}$$

Once equation (2) is solved, the Kelvin model can be used to simulate car to pole collisions. It should also be noted that mass, m, for the Kelvin model is the same as the mass of the car. Once the mass is known, using equation (2) with the initial impact velocity as input and accelerometer data as output, the coefficients c and k can be calculated.

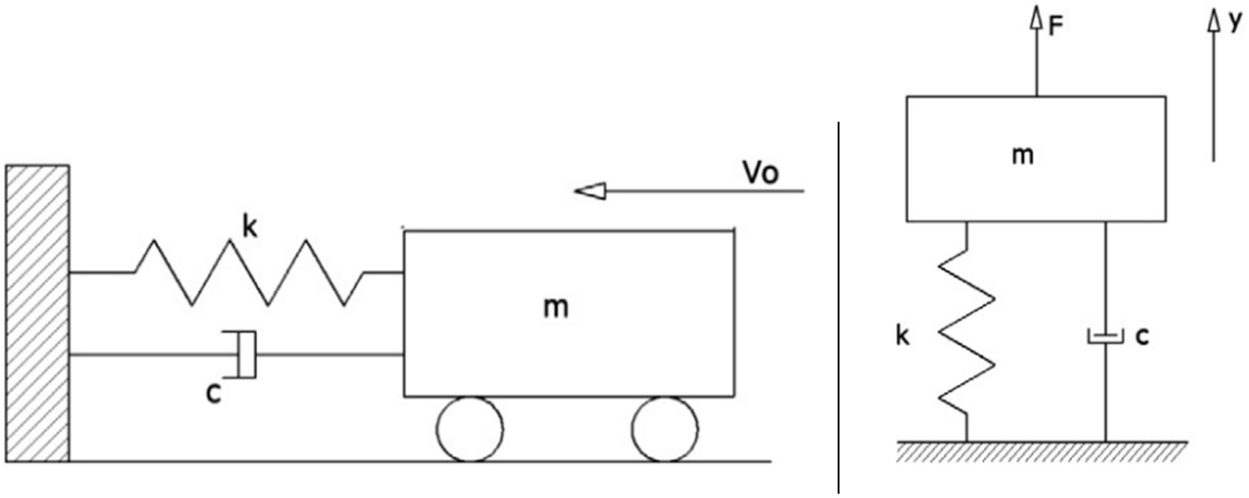

Figure 2-1: (a) Kelvin Model (Pawlus, 2011), (b) mass-spring-damper model (Pawlus, 2011)

In addition to the Kelvin model, the Maxwell model is also a popular lumped parameter model for vehicle crash modeling. The Maxwell model, as shown in figure 2-2, is a mass-spring-damper system with the spring and damper connected in series. The EOM for displacement of mass *m* and zero-mass *m'* are given from Pawlus et al. as follows:

$$m\ddot{d} = -c(\dot{d} - \dot{d}')$$

$$m'\ddot{d}' = c\left(\dot{d} - \dot{d}'\right) - kd'$$

By differentiating the equations above with respect to time and setting $m' = 0$, and then combining the resulting equations, the equation of motion (EOM) can be obtained. The EOM for a Maxwell model is shown in equation (3) as follows:

$$\dddot{\boldsymbol{d}} + \frac{\boldsymbol{k}}{\boldsymbol{c}}\ddot{\boldsymbol{d}} + \frac{\boldsymbol{k}}{\boldsymbol{m}}\dot{\boldsymbol{d}} = \mathbf{0} \tag{3}$$

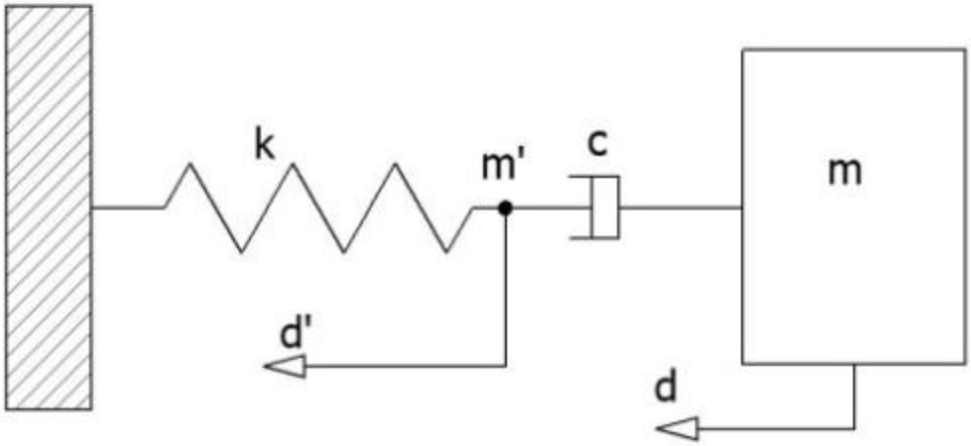

Figure 2-2: Maxwell model - m' designates zero-mass (H. R. K. Witold Pawlus, Kjell G. Robbersmyr, 2010)

The mass in this model will not rebound from the impacted obstacle, meaning that it can account for the crumbling of the crash structure. The dominating value in determining whether or not the mass will rebound is the damping coefficient *c*. When the mass is less than a certain critical value *c'*, then the mass will asymptotically approach the obstacle and when it is higher, there will be dynamic crush at a finite time (H. R. K. Witold Pawlus, Kjell G. Robbersmyr, 2010).

For both models mentioned above, the method to calculate the spring and damper coefficients follows the same logic. The inputs, initial impact velocity for both models and the impact force for the Kelvin model, and the output, accelerometer data, are used to determine the coefficients. This is done by iterating the coefficients till a desirable output is achieved. However, the problem with this method is that the coefficients are dependent on the testing scenario. If, for example, this system was to be used to determine crush for different crashes, then for every single crash estimate desired, there would need to be

different coefficients. That means that for every single scenario, there would need to be different testing data for each scenario. Additionally, for every single vehicle model that uses a lumped parameter mode, there would need to be different training data for that model. This causes for an overall system that is not versatile, nor is it easily adjustable for new scenarios. These problems were not originally anticipated as LPMs for crash modeling were developed for testing environments and not real-world scenarios. Thus, a more robust approach is desired, and based on literature search, it is a data-based approach as shown below in section 2.1.3.

2.1.3 Data Based Approach to Vehicle Crash Modeling

As previously mentioned, lumped parameter models (LPM) are limited by the testing scenarios used to determine the model coefficients. There are methods to use autoregressive models to predict time series data that can be used to determine LPM coefficients (H. R. K. Witold Pawlus, and Kjell G. Robbersmyr, 2013). What Pawlus et al. have developed is methodology to simulate crashes using multibody models as shown in figure 2-3, which creates inputs for the previously discussed LPMs. This means that LPM coefficients can be developed using simulated data, thus decreasing the number of experimental crash tests needed.

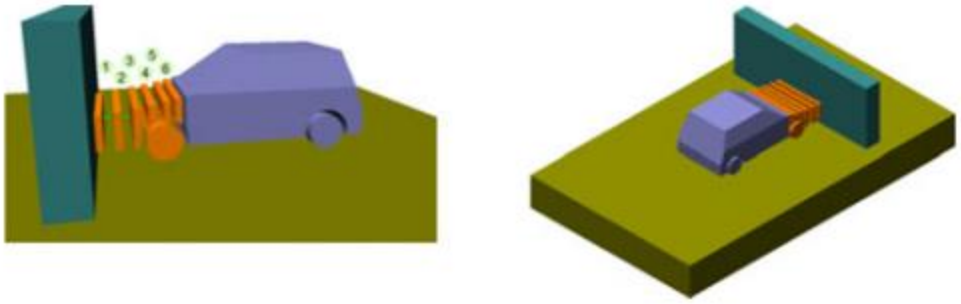

Figure 2-3: Multibody Model (H. R. K. Witold Pawlus, and Kjell G. Robbersmyr, 2013)

Simulated crashes have data generated by different LPMs of different impact scenarios. Figure 2-3 shows a front impact scenario, where the front is divided into 6 undeformable components connected by a spring and a damper. The coefficients are determined to match a set reference data through trial and error, which then gives a virtual copy of the reference crash test. This model can only simulate output in one direction, longitudinal, however, it is much cheaper and faster than experimental testing. The output from the virtual model is used to make the Kelvin or Maxwell models more reliable (H. R. K. Witold Pawlus, and Kjell G. Robbersmyr, 2013).

A data-based approach reduces the need for experimental crash tests, but it does not eliminate it. With LPMs, it is impossible to produce an accurate model without experimental testing. It is possible to determine crush, as done with LPMs, by simply analysing the crash pulse analysis as discussed in the next section.

2.1.4 Crash Pulse Analysis

Access to accelerometer data during a crash test means the car's motion can be described in detail. As previously discussed, by integrating the car's deceleration, velocity and displacement can be obtained (Pawlus, 2011). An example of this is shown in figure 2-4 from the work of Pawlus et al. In figure 2-4, the blue curve denotes the acceleration

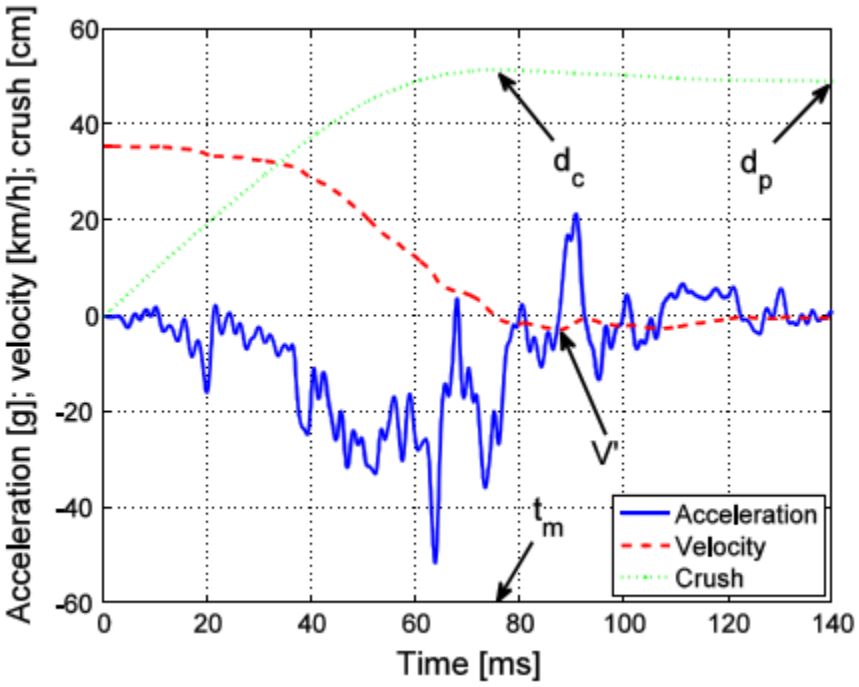

Figure 2-4: Car's Kinematics (H. R. K. Witold Pawlus, and Kjell G. Robbersmyr, 2013)

signal acquired from the test vehicle. Integrating that with the initial impact velocity gives the red curve, the rebound velocity *V'*. Integrating the rebound velocity gives the dynamic crush or crush is depicted as point d_c and the time it occurs at is t_m with d_p being the permanent deformation. In chapter 3, permanent deformation is not considered, instead crush is used. This is because the cash test data is inconsistent, therefore, the permanent deformation prediction is not accurate. For the purposes of this thesis, crush is calculated by crash pulse analysis rather than LPM or FEM. Doing so provides a much simpler approach to crash modeling.

2.2 ADAS Output

There is limited literature available on the type of data expected as ADAS output as each vehicle manufacturer would have a different method. Therefore, a brief overview of radar and ultrasonic sensors is provided rather than information on the data itself. Chapter 3 has more information regarding the format of the data, this information was collected from a 2016 Ford Fusion Energi. Data was accessed from the controller area network (CAN) bus using an OpenXC dongle, a opensource dongle available to purchase on the consumer market.

2.2.1 Radar and Ultrasonic Sensor

Radar systems emit microwaves and measure the change in frequency of the reflected wave as defined by the Doppler effect. The output from the radar is the speed and distance between the vehicle and the object within the radar's range. Depending on when a car was introduced, it may be that its radar only outputs the difference in speed between the car and the object as older radar systems did not show distance. One of the benefits of radar is that it is not affected by rain or foggy weather like light-based systems would be. There are three types of radar systems, short range, medium range, and long range as shown below in table 2-1. Adaptive cruise control (ACC) systems use long range radar with short and medium range radar being used for cross traffic alert and blind-spot detection (Vipin Kumar Kukkala, 2018). For this thesis, ACC was the only ADAS system considered, although, in the data described in chapter 3, a medium range radar was used.

Table 2-1: Radar Systems (Vipin Kumar Kukkala, 2018)

Radar Type	Range
Short Range	0.2-30 meters
Medium Range	30-80 meters
Long Range	80-120 meters

Ultrasonic sensors use sound waves to measure distance and are mainly used for detecting objects very close to the vehicle. Some uses of ultrasonic sensors include use for parking sensors, which then results in its use for automatic parking and parallel park assist (Vipin Kumar Kukkala, 2018). As shown in chapter 1, parking sensors are located towards the front and rear of the vehicle. For this thesis, parking sensors are used to detect the impact location, more information on their use is given in chapter 3.

2.3 Principle Degree of Force

Principle degree of force (PDOF) is the direction of the crash impulse and can be derived using accelerometer based measurements. PDOF can be used to determine impact side, however, as shown in figure 2-5 a 45° impact could easily be a front impact or a side impact. Due to the possibility of predicting multiple impact sides, PDOF is only used for

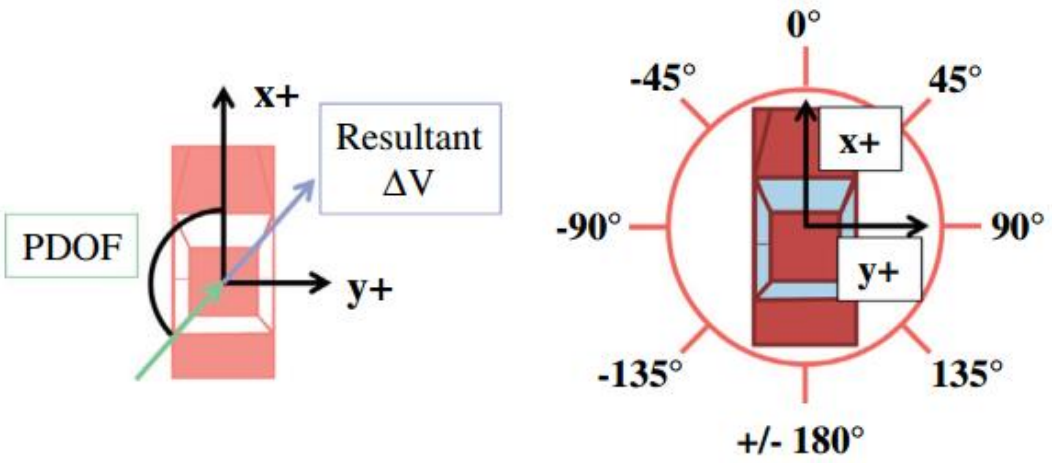

Figure 2-5: PDOF Angle (Kristofer D. Kusano, 2012)

side impacts as there is minimal parking sensor coverage on the side. Kusano and Gabler examined 146 real world crashes using PDOF in the event data recorder (EDR) to determine the accuracy of PDOF calculations. They used equation 4 to determine the PDOF and from that, they concluded that PDOF estimates were within 10° of the angles measured during crash testing.

$$PDOF = tan^{-1}\left(\frac{\Delta V_y}{\Delta V_x}\right) = tan^{-1}\left(\frac{a_y}{a_x}\right) \quad (4)$$

2.4 Conclusion

The literature review covered several different methods of crash modeling and provided an overview of the ADAS sensors used for this thesis. The traditional approach to crash modeling would require the use of finite element methods or lumped parameter models, however, for this thesis, crash pulse analysis will be used. Crash pulse analysis does not require a model to accompany it and since crash acceleration data is used for this thesis, using crash pulse analysis to determine crush makes sense. That leads to the ADAS section of the literature review, where radar and ultrasonic sensors were covered. These sensors will be used to determine the impact location on the vehicle along with the PDOF where necessary. More information on ADAS sensor use and PDOF is given in chapter 3.

CHAPTER 3. METHODOLOGY

The literature review showed that there are multiple crash modeling methods available. In this chapter, the focus will be on crash pulse analysis and its use in crash modeling by crush prediction. Additionally, this chapter will also cover the use of ADAS sensor data and PDOF to determine impact location around the car. The methodology below begins with an overview of the entire algorithm to predict impact damage and then provides more details for each step in the overview. It is also important to note at this point how impact damage is defined. For impact damage, the final goal is to be able to determine which parts are damaged on the car.

3.1 Overview of Combined Algorithm

The goal of this algorithm is to predict which parts are damaged on impact. To accomplish this, accelerometer data and ADAS (parking sensor and radar) data are used as inputs. Descriptions of the input data are provided below in section 3.1.1. A high level flowchart is shown in figure 3-1. From the figure, determining crush and determining location are two different processes. The commonality between them is input data, they both use accelerometer data and the location determination process also takes ADAS data as input. From there, the outputs are combined and used to determine which parts are damaged on the car.

3.1.1 Description of Input Data

The input data from the algorithm is the accelerometer data, parking sensor data, and radar data. From the literature review, crush is determined using crash pulse analysis.

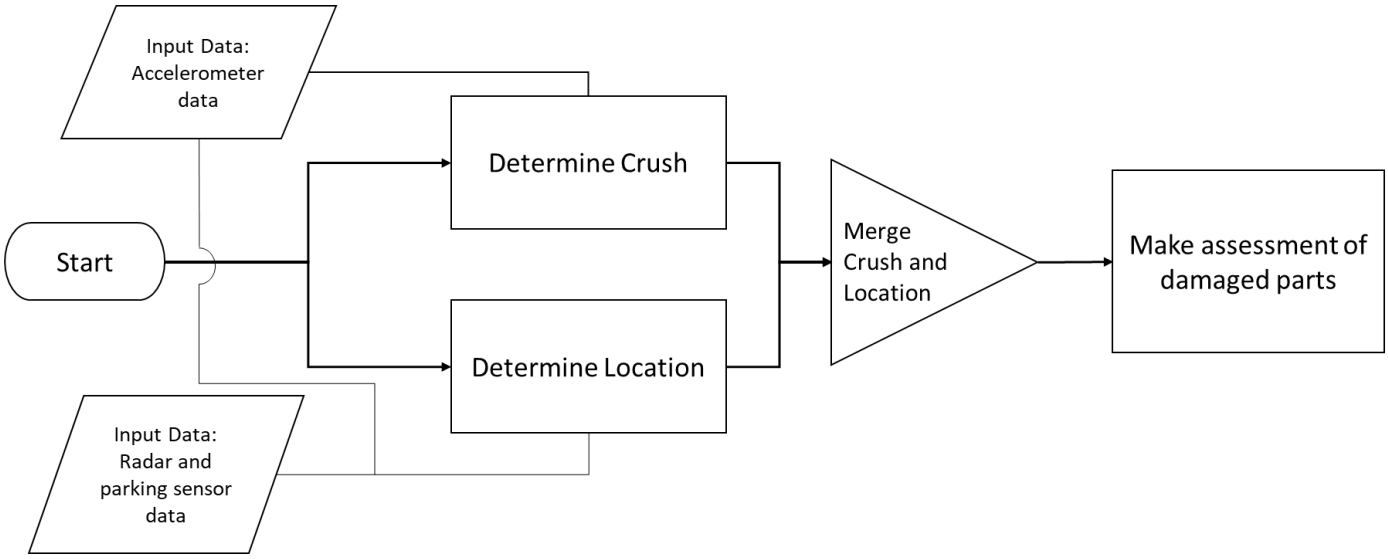

Figure 3-1: High Level Algorithm Flowchart

Characteristics for the data used for analysis are shown below in table 3-1. To analyse the crash pulse, the accelerometer data must span from the point of impact to the end of impact. If the point of impact is at 0 seconds, then it can be said that the accelerometer data spans from 0 to 2 seconds. It is assumed that the any impact will be over within two seconds. If it can be shown that the impact takes longer than two seconds, then this number can be adjusted. The accelerometer data used for analysis in chapter 4 is in *[g]*, it can also be used as *[meters/second^2]*, but if it is any other unit, the data must be converted to either of the units mentioned in table 3-1.

The ADAS data used for analysis must come from immediately before the crash. For this analysis, it was taken from 2 seconds before the impact to the point of impact or 0 seconds. The 2 second figure was chosen arbitrarily; it can be changed if there is a reason to do so. Otherwise, it is better to leave it at 2 seconds as a larger value could result in unnecessary data being captured by the sensor. Table 3-1 also shows that the parking sensor

data is unitless. This is due to the test vehicle used for this thesis, a 2016 Ford Fusion Energi, having unitless parking sensor data.

In section 2.2.1, it is given that radar output data is distance and the difference in speed between the car and the incoming object. It is also stated that some older car models only output the difference in speed between the car and the incoming object. For this thesis, the vehicle used to study sensor data was a 2016 Ford Fusion Energi. Using an OpenXC dongle and open source code, the data from the car's sensors can be accessed. From that information, it is known that the 2016 Ford Fusion Energi radar only outputs the speed between the car and the incoming object. So, for this analysis, the only radar data used was the difference in velocity.

Table 3-1: Input Data Parameters

Sensor	Time Span	Units
Accelerometer	0 to 2 seconds	$[g]$ or $[meters/second^2]$
Parking or Ultrasonic Sensor	-2 to 0 seconds	Unitless
Radar	-2 to 0 seconds	$[km/hr]$

3.2 Crush Prediction Algorithm Challenges and Design

In this section, the challenges associated with determining crush using crash pulse analysis are discussed. Additionally, the solutions to those challenges and the flowchart for

crush determination is also discussed. Figure 3-2 below contains the crush prediction algorithm flowchart. The first step is to determine the impact side using the accelerometer data, why this is done is explained in the challenges sub-section. Then, once the impact side is determined, the crush can be determined using the correct accelerations signal, either lateral or longitudinal.

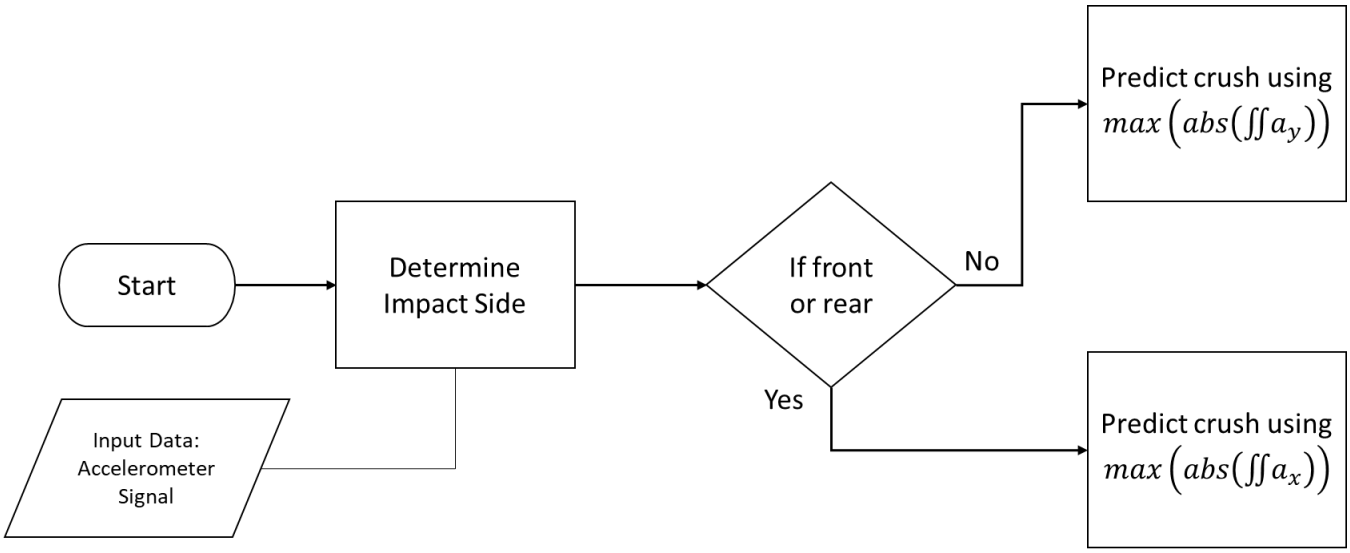

Figure 3-2: Crush Prediction Flowchart

3.2.1 Challenges

From the literature review and figure 3-2, crash pulse analysis to determine crush requires data from the accelerometer. From the work of Pawlus et al., it is seen that the pulse analyzed is for a front impact. This means that the longitudinal acceleration is used for crash pulse analysis. However, for real world data, both longitudinal and lateral data is obtained. Which raises the question, should the longitudinal or lateral acceleration data be used for crush prediction? This information is given for a crash test, but not for real world crashes. So, the algorithm in figure 3-2 has a process to determine the impact side. Once

the impact side is determined, either a_y or a_x can be used to determine crush. So, for a front or rear impact, the x-axis data is used. This is similar to what is shown in figure 2-5, with the only difference being that the y-axis is flipped. This change is shown in figure 3-3. The reason this is done is to align better with the testing data used, which is described in section 3.5.

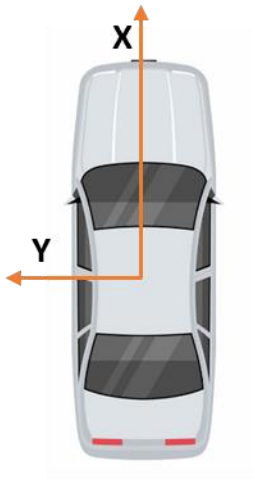

Figure 3-3: Axis Description

3.2.2 Determining Impact Side

To determine the impact side, the only sensor information needed comes from the accelerometer. This can be done by using looking at a basic kinetic energy equation as follows:

$$KE = \frac{1}{2}mv^2$$

The kinetic energy equation defines the total energy that would need to be dissipated during the crash. The process to determine the impact side is shown in figure 3-4. The flowchart

in figure 3-4 uses the accelerometer data as described in table 3-1 with the initial impact velocity v_i known from the car during impact. Additionally, instead of using the velocity, displacement is used in the logical blocks to determine impact side. The reason displacement is used is that whichever direction the impact is in will have the highest absolute crush. That means that the crush in the x-direction will be higher than the y-direction if it is a front or rear impact and vice versa for a side impact. To determine crush, the only information needed is the impact axis, so knowing front/rear or side is enough to determine crush. The steps following that are done anyways for the location detection as described below.

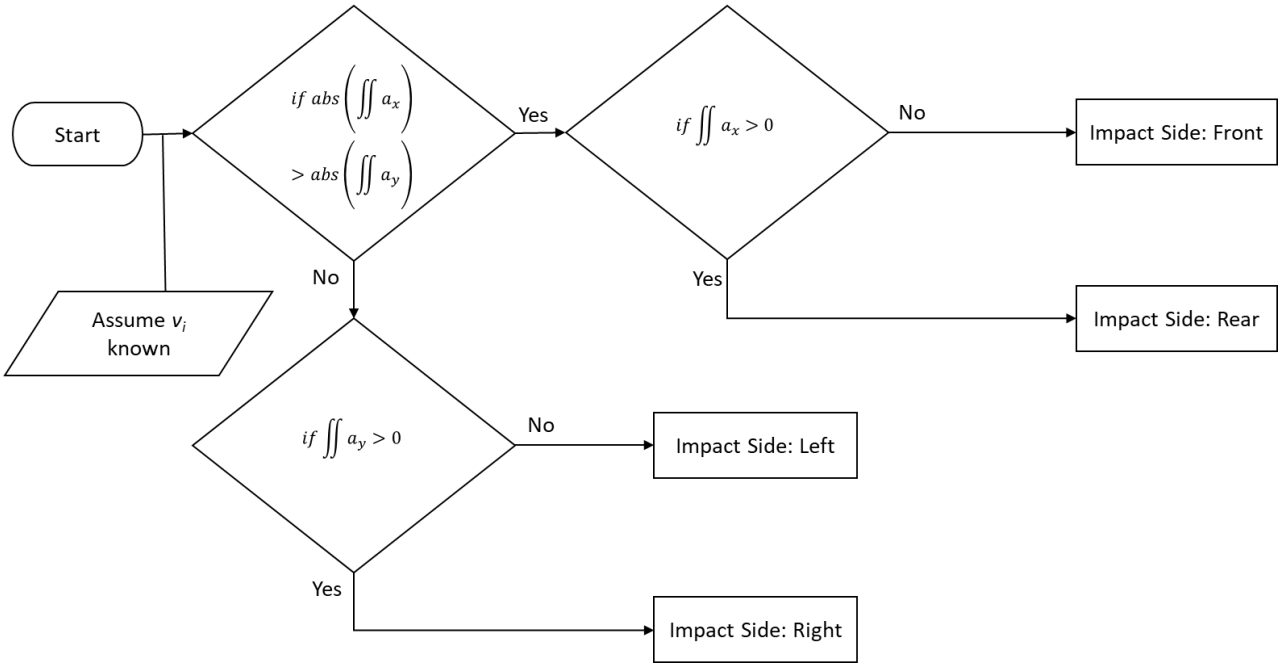

Figure 3-4: Flowchart to Determine Impact Side

For location detection, it is important to know which sensors have relevant data. It is possible that during a front impact, rear parking sensors could have an object in their range. So, by using the second part of the flowchart in figure 3-4, the exact impact side can

be determined. This is done by considering the positive and negative directions on each axis as shown in figure 3-3. For example, during a front impact, the crush will be negative and positive for a rear impact. For a left impact, the crush will be negative and for a right impact, the crush will be positive. Knowing the impact side ensures that the right ADAS sensors are being considered when determining the impact location. More on this is given in section 3.3.

3.2.3 Determining Crush

Determining crush is the easiest of the crash modeling techniques described in the literature review. The process is simple, once the impact zone is known as front/rear or side, then the corresponding accelerometer data along with the initial impact velocity can be used to determine crush. Integrating the acceleration signal gives velocity, and integrating velocity gives displacement. Crush is the point d_c in figure 2-4, the point of maximum displacement. So, for this case, using the final blocks of figure 3-2 or equation 5 provides the crush.

$$crush = max\left(abs\left(\iint a\right)\right) \tag{5}$$

3.3 Location Prediction

In this section, the logic used to predict the impact location around the car will be discussed. The basics of this logic is shown in the flowchart in figure 3-6. Using the logic shown in figure 3-4 and discussed in sub-section 3.2.2, the impact side needs to be determined. Once that is done, then the logic in figure 3-4 can be used to determine which

sensors contain the relevant data. Approximate locations of parking sensors and radar is shown in figure 3-5 with each parking sensor labeled. For a front impact, the radar and front parking sensors need to be used and for a rear impact, the rear parking sensors need to be used. For side impacts, the process is slightly different due to the lack of side facing parking sensors. So, for side impacts, if the impact is in the side facing sensor's range, then the sensor data is used, otherwise, PDOF is calculated and the angle is used to determine the closest impact zones (discussed in section 3.3.1).

Figure 3-5: ADAS Sensor Locations

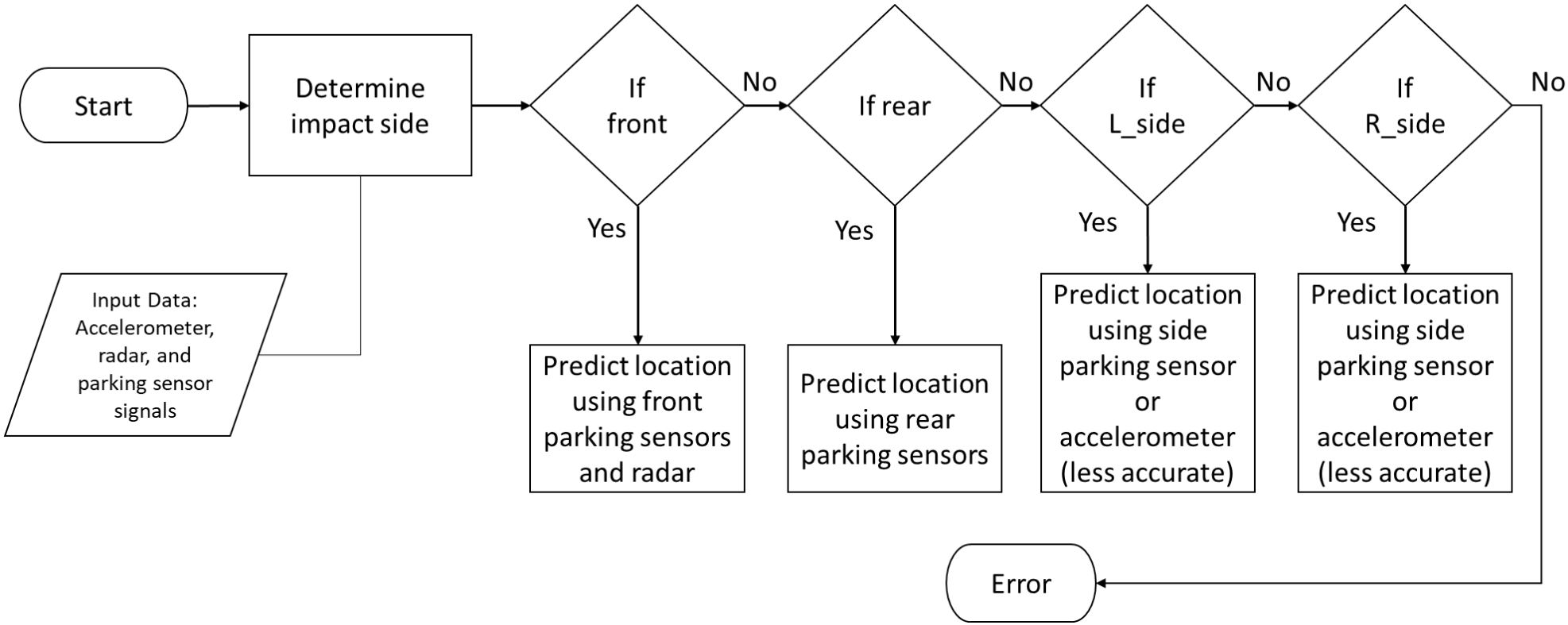

Figure 3-6: Location Prediction Flowchart

3.3.1 Introduction to Impact Zones

From figure 3-5, for front and rear impacts, there is an acceptable amount of sensor coverage. However, for side impacts, there is only one parking sensor on each side, S1 on the right side and S4 on the left side. From figure 3-6, for side impacts, the side facing sensors are used, if the relevant sensor does not show an impact, then the accelerometer is used. The accelerometer is used to determine PDOF, which then can be used to extrapolate the impact area. However, for all scenarios, the exact impact zones have not been shown. Figure 3-7 shows the impact zones around the car with each zone being labelled 1 through 22. Each zone was selected to be easy to deploy throughout the entire process in figure 3-1. In areas with acceptable sensor coverage, front and rear, the impact zones were selected to make it easier to predict the impact zone first and then the parts damaged. For all other areas, the impact zones are divided up according to where the exterior panels are located.

Table 3-2 shows the parts located in each impact zone for a 2016 Ford Fusion Energi. As discussed before, the reason a 2016 Ford Fusion was used was that this vehicle was available for testing during this thesis. Each of the zones were measured to give an approximate location and the crush associated with each part is also given in section 3.4.

At this time, it is also convenient to explain the terminology used in the latter sections. When it is said that an object is “seen” or “visible” on a specific sensor, it is meant that the object is generating a positive output for that sensor.

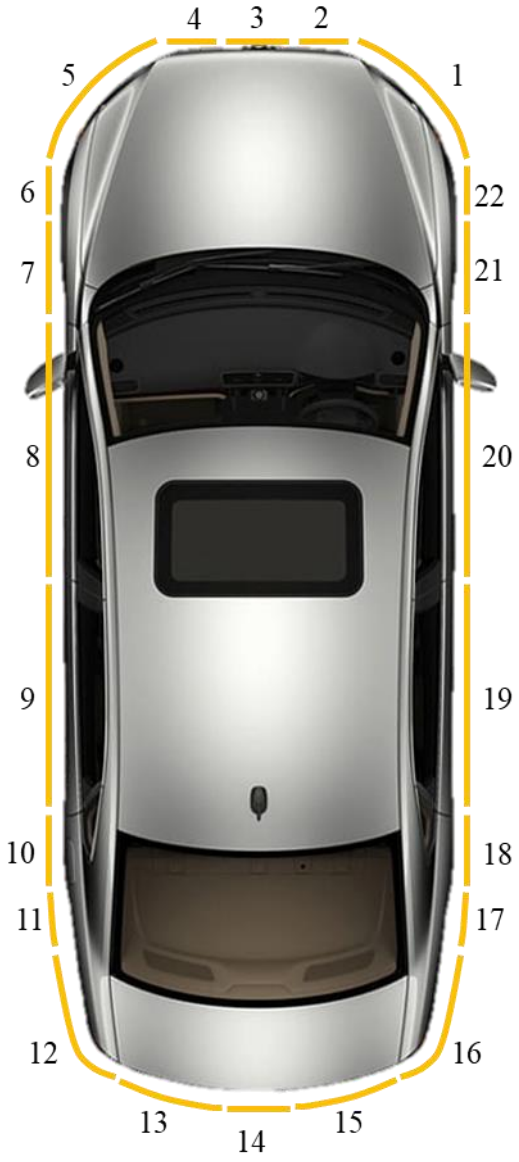

Figure 3-7: Impact zones around the car

Table 3-2: Parts in different impact zones

Impact Zone	Side	Parts in Impact Zones
1	Front Right Corner	Headlight, fog light, and bumper
2	Front	Bumper, radiator, and hood
3	Front	Bumper, radiator, and hood
4	Front	Bumper, radiator, and hood
5	Front Left Corner	Headlight, fog light, and bumper
6	Left Side	Front fender and bumper

Table 3-2 continued

7	Left Side	Front fender and wheel
8	Left Side	Front door
9	Left Side	Rear door
10	Left Side	Rear fender and wheel
11	Left Side	Rear bumper and fender
12	Rear	Taillight and bumper
13	Rear	Bumper and trunk
14	Rear	Bumper and trunk
15	Rear	Bumper and trunk
16	Rear	Taillight and bumper
17	Right Side	Rear bumper and fender
18	Right Side	Rear fender and wheel
19	Right Side	Rear door
20	Right Side	Front door
21	Right Side	Front fender and wheel
22	Right Side	Front fender and bumper

3.3.2 Front Impacts

There are two different types of front impacts that can occur, a full-frontal impact or a partial impact at the front. A full-frontal impact would mean an impact in zones 1, 2, 3, 4, & 5 from figure 3-7 and a partial impact at the front could be at any one or more zones in the front. Figure 3-8 provides a flowchart to the logic used to determine the front impact zone. From the flowchart, if the impact is only visible on radar, then it is in zone 3. If the incoming object is visible on sensors S2 and S3 at the same time, and visible on radar, then it is an impact in zones 1, 2, 3, 4, & 5. If the object is visible on radar and S2 at the same time point, then it is an impact in zones 2 & 3. If it is visible on radar and S3 at the same time point, then it is impact zones 3 & 4. If the object is last visible on S2, then it is a impact in zone 2, and if it is last visible on S3, then it is a impact in zone 4. Finally, if the object is last visible on the radar, then it is an impact in zone 3.

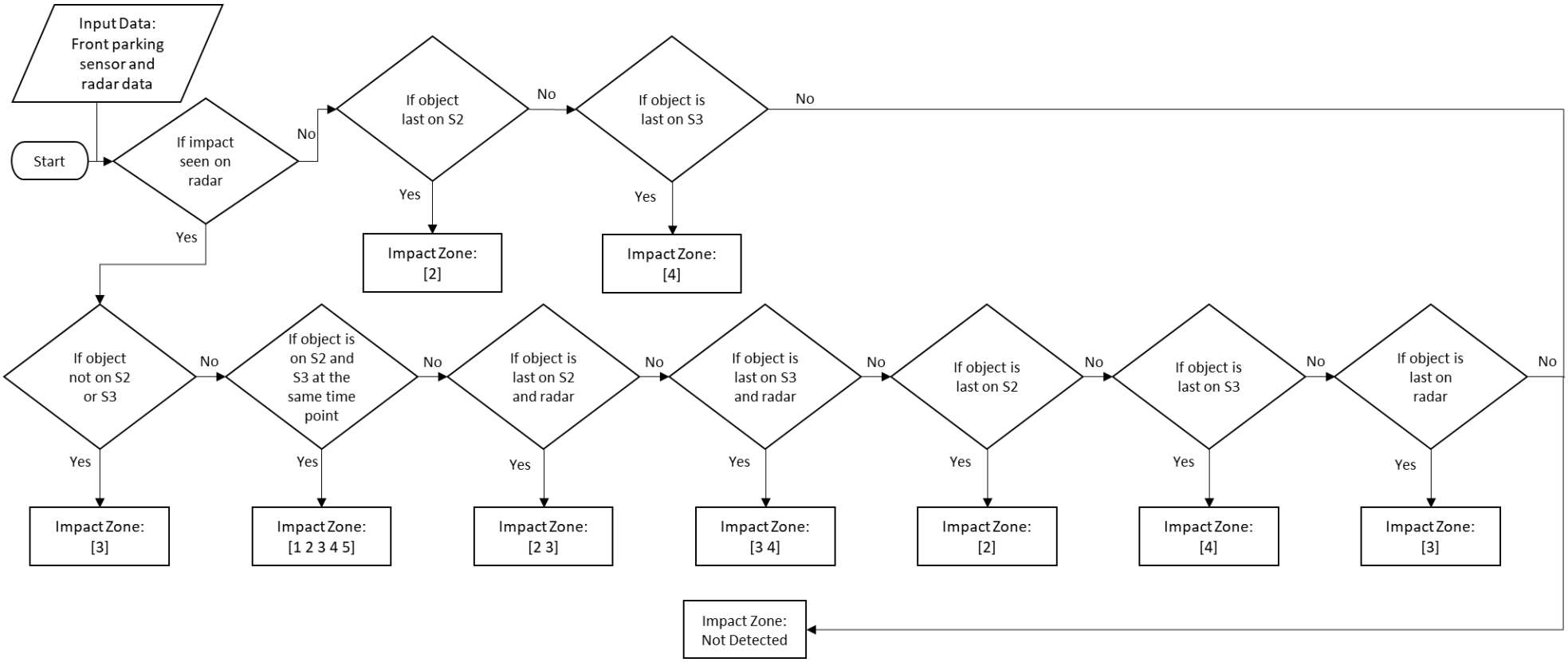

Figure 3-8: Flowchart to determine front impact zones

For front impacts, if an incoming object is not visible on radar at all, then there are one of two impact scenarios from ADAS data. From figure 3-8, if an object is not visible on radar and is last seen on S2, then it is an impact in zone 2. If the object is not visible on radar and is last seen on S3, then it is an impact in zone 4. Finally, if the impact is not detected, then sub-section 3.3.5 applies and table 3-3 is used is used to obtain impact zones.

3.3.3 Rear Impacts

Rear impacts follow a very similar logic to that of frontal impacts, the only difference is that there is no rear radar included in this logic. This may be contradictory to the literature in section 2.2, but as mentioned earlier, for this thesis, a 2016 Ford Fusion Energi was used for testing and it did not come with a rear radar. Figure 3-9 shows the logic used for rear impact zone location in a flowchart. From that, if the object is last seen on S6 and S7, then the impact zone is 14 from figure 3-7. If it is last seen on S5, then the impact zones are 12 & 13, and similarly, if it is last seen on S8, then the impact zones are 15 & 16. If the object is last seen on S6, then it is not a simple classification. For an object last seen on S6, if after S6, it is last seen on S5, then the impact zones are 13 & 14. If, however, after S6, it is last seen on S7, then the impact zone is 13. Similarly, to S6, if an object is last on S7, then the classification is not simple. This can be found in figure 3-9.

Lastly, if an on S5, S6, S7, and S8 at the same time point, then the impact zones are 12, 13, 14, 15, & 16 or a full rear impact. Similarly, to front impacts, if an object is not seen on any rear parking sensor, then the impact zone cannot be determined. In this case, sub-section 3.3.5 applies and table 3-3 is used to obtain impact zones.

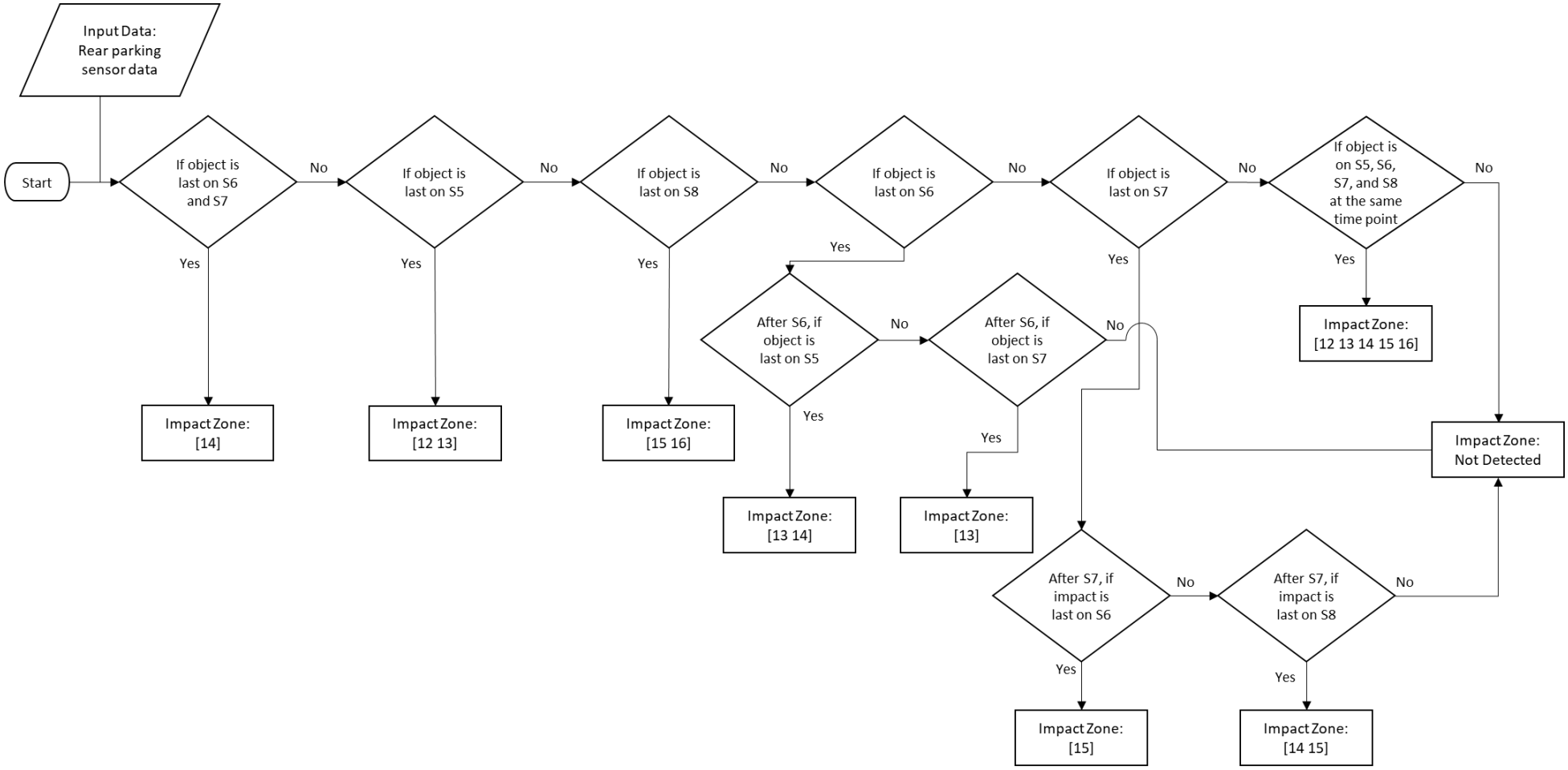

Figure 3-9: Flowchart to determine rear impact zones

3.3.4 Side Impacts (with ADAS data)

Detecting side impacts using ADAS data is much simpler in comparison to front or rear impacts due to there only being two side facing sensors. Figure 3-10 shows the logic used to detect side impacts. If the object is seen on S1, then the impact zone is 22. Similarly, if the object is seen on S4, then the impact zone is 6. And if neither S1 nor S4 register the incoming object, then the impact side cannot be determined. In the case that the impact side cannot be determined, then section 3.3.5 applies and table 3-3 is used to obtain impact zones.

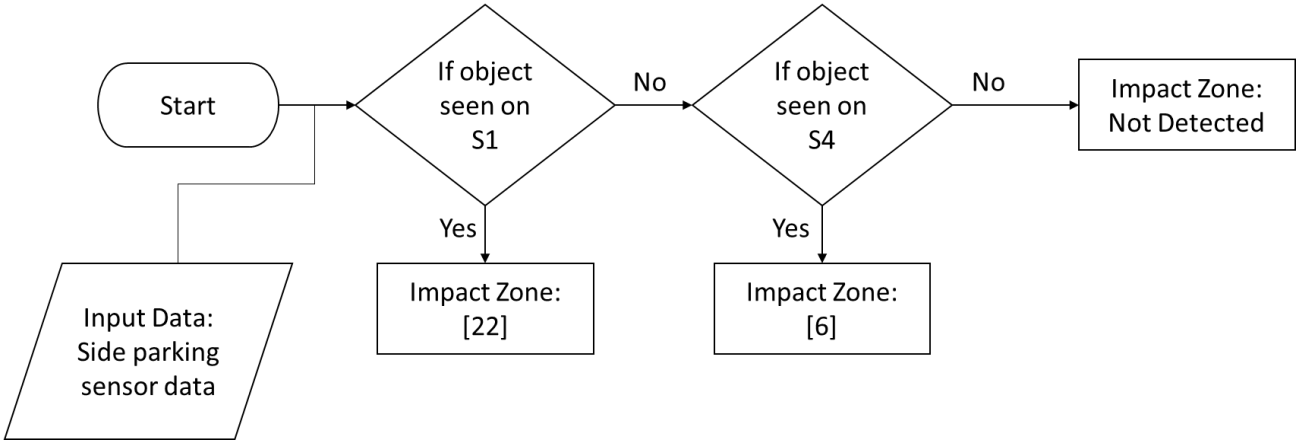

Figure 3-10: Flowchart to determine side impact zones

3.3.5 Side Impacts (without ADAS data)

For side impacts where the impact is not in sensors S1 and S4 from figure 3-5, PDOF needs to be used to determine impact zone. It is possible that this impact is anywhere on the car, not just a side impact. This could be a front impact if it is outside the range of the radar and too fast for the parking sensors. It could be a rear impact if it is too fast for the parking sensors. However, no matter what the impact side is, the approach is the same.

Determine the PDOF using equation (4). Then use the vehicle's dimensions to determine the coordinates of the impact. Once this is done, the last step is just to see which impact zone the coordinates are in. The coordinates inches for a 2016 Ford Fusion Energi are given in table 3-3 below.

Table 3-3: Impact Zone Coordinates

Impact Zone	x-axis range [inches]	y-axis range [inches]
1	[96 96]	[-36.5 -20.5]
2	[96 96]	[-20.5 -5]
3	[96 96]	[-5 5]
4	[96 96]	[5 20.5]
5	[96 96]	[20.5 36.5]
6	[71 96]	[36.5 36.5]
7	[42 71]	[36.5 36.5]
8	[-1 42]	[36.5 36.5]
9	[-44 -1]	[36.5 36.5]
10	[-44 -69]	[36.5 36.5]
11	[-69 -96]	[36.5 36.5]
12	[-96 -96]	[29.5 36.5]
13	[-96 -96]	[5 29.5]
14	[-96 -96]	[-5 5]
15	[-96 -96]	[-29.5 -5]
16	[-96 -96]	[-36.5 -29.5]
17	[-69 -96]	[-36.5 -36.5]
18	[-44 -69]	[-36.5 -36.5]
19	[-44 -1]	[-36.5 -36.5]
20	[-1 42]	[-36.5 -36.5]
21	[42 71]	[-36.5 -36.5]
22	[71 96]	[-36.5 -36.5]

3.4 Determining Parts Damaged

In this section, the focus will be on taking the outputs from sections 3.2 and 3.3 and converting them into actual parts damaged on a car for a given impact scenario. As a reminder, the output from section 3.2 is the crush during the impact and the output from section 3.3 is the impact zone where that crush occurred. The impact zones are shown in figure 3-7 and the parts corresponding to each zone are in table 3-2. Using crush and impact zone, the parts damaged can be determined using the process in figure 3-11. The process shown is simple, for a given impact zone, determine if the crush is high enough to damage a part. Impact zones may have multiple parts, with a possibility of one part being placed behind another. In this case, certain parts will have a minimum crush required to cause damage. This information is given below in table 3-4. Using the information in table 3-4, for each impact zone, determine if the crush meets the threshold given for each part. If the threshold is met, then the part is damaged, and the process repeats until there are no more parts left.

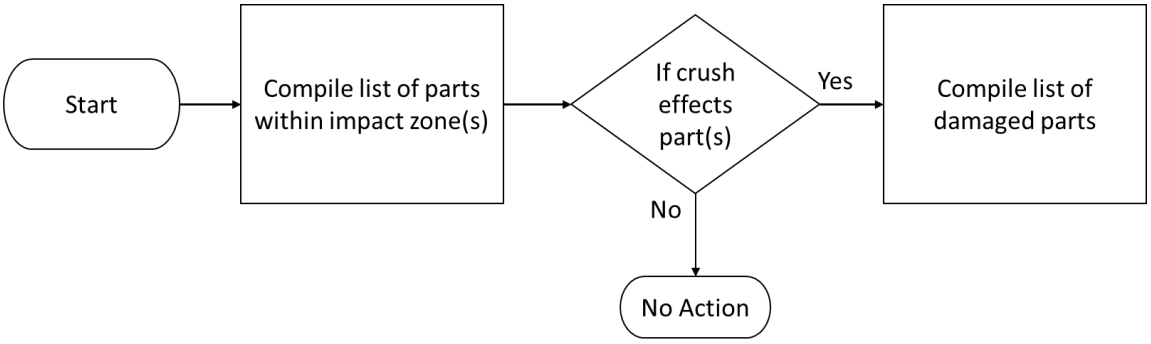

Figure 3-11: Flowchart to determine parts damaged

Table 3-4: Crush for parts in different impact zones

Impact Zone	Part	Min Crush [cm]	Max Crush [cm]
1	Headlight (Right)	0.0	53.3
1	Fog light (Right)	10.2	43.2

Table 3-4 continued

1	Front Bumper (Right)	0.0	58.4
2	Front Bumper (Mid)	0.0	12.7
2	Hood	12.7	114.3
2	Radiator	12.7	27.9
3	Front Bumper (Mid)	0.0	12.7
3	Hood	12.7	114.3
3	Radiator	12.7	27.9
4	Front Bumper (Mid)	0.0	12.7
4	Hood	12.7	114.3
4	Radiator	12.7	27.9
5	Headlight (Left)	0.0	53.3
5	Fog light (Left)	10.2	43.2
5	Front Bumper (Left)	0.0	58.4
6	Front Fender (Left)	0.0	17.8
6	Front Bumper (Left)	0.0	39.4
7	Front Fender (Left)	0.0	17.8
7	Front Wheel (Left)	0.0	20.3
8	Front Door (Left)	0.0	17.8
9	Rear Door (Left)	0.0	17.8
10	Rear Fender (Left)	0.0	17.8
10	Rear Wheel (Left)	0.0	20.3
11	Rear Bumper (Left)	0.0	17.8
11	Rear Fender (left)	0.0	17.8
12	Taillight (Left)	0.0	40.6
12	Rear Bumper (Left)	17.8	63.5
13	Rear Bumper (Mid)	0.0	17.8
13	Trunk	0.0	50.8
14	Rear Bumper (Mid)	0.0	17.8
14	Trunk	0.0	50.8
15	Rear Bumper (Mid)	0.0	17.8
15	Trunk	0.0	50.8
16	Taillight (Right)	0.0	40.6
16	Rear Bumper (Mid)	17.8	63.5
17	Rear Bumper (Right)	0.0	17.8
17	Rear Fender (Right)	0.0	17.8
18	Rear Fender (Right)	0.0	17.8
18	Rear Wheel (Right)	0.0	20.3
19	Rear Door (Right)	0.0	17.8

Table 3-4 continued

20	Front Door (Right)	0.0	17.8
21	Front Fender (Right)	0.0	17.8
21	Front Wheel (Right)	0.0	20.3
22	Front Fender (Right)	0.0	17.8
22	Front Bumper (Right)	0.0	39.4

3.5 Obtaining Testing Data

So far in chapter 3, an algorithm that could be used to determine which parts are damaged during a crash is discussed. Section 3.2 provides information on predicting crush, section 3.3 provides information on predicting impact zones, and section 3.4 combines both of those to determine which parts are damaged on the car. In theory, the algorithm makes sense, however, it needs to be proved. So, this section focuses on the process of obtaining data to test the algorithm and chapter 4 will discuss the results from these tests.

3.5.1 Data for Crush Prediction

As discussed in section 3.2, crush prediction requires accelerometer data as an input. There are two ways to get this data, one is from crash tests and the other is by simulating it. To simulate the data, the lumped parameter modeling method discussed in 2.1.3 can be used. However, there are numerous crash tests conducted each year by the Department of Transportation for new cars where the crash data is available in the public domain. So, to prove the algorithm laid out in this chapter, data from the National Highway Traffic Safety Administration (NHTSA) is used. NHTSA has a vehicle crash test database where they publish data for new and old crash tests. NHTSA conducts front, rear, and side

impact crash tests. However, they only instrument their side impact crash tests with accelerometers. Additionally, for the side impact tests, there are two impact scenarios, 32 [kph] and 60 [kph]. The 32 [kph] impact is a vehicle into pole test where the test vehicle is slung sideways into a pole at 32 [kph]. The second impact type, 62 [kph], is a side impact with a deformable barrier. For this scenario, a deformable barrier impacts a stationary test vehicle at 62 [kph]. The two tests mentioned were the only instrumented crash tests on NHTSAs database, thus, the only two cases used.

3.5.1.1 Challenges

There are two main challenges faced when using the NHTSA data. The first one being that only side impact crashes are instrumented. This results in only being able to use side impact data to check the crush prediction part of the algorithm. The second problem is to do with the data itself. By observing the data downloaded for the crush analysis, it became clear that the data ended inconsistently. Some datasets ended immediately after the impact, while some continued for another second or two. This directly affects the crush due to the way it is calculated. The crush is calculated by integrating the accelerometer signal to obtain displacement. So, if the signal continues longer than needed, and if it is noisy, then this could cause an error in the crush measurements.

The data ending inconsistently was causing an issue in the results, so to decrease the error, a cut-off point is found in the data. This is easy to do by eye, but the challenge was to create a method to do this automatically. The cut-off point was found by first using a low pass filter to decrease the effect of noise in the data. Then, using the findpeaks() function in MATLAB, every local maxima was found. From the list of local maxima, the

highest value was used as a threshold. After this, going back through the data, when the local maxima dropped below 15% of the threshold, then that would be the cut-off point. Chapter 4 will show that the effect of using a cut-off point by comparing the error with and without a cut-off point.

3.5.2 Data for Impact Zone Prediction

As discussed above, accelerometer data from crash tests is available on the public domain. However, to predict the impact zone, ADAS data is required, and from a literature search, it became clear that there is no ADAS data from crash tests available on the public domain. So, the only solution left was to simulate ADAS data for different impact scenarios. This was done using assumptions about sensor data that would be obtained from a 2016 Ford Fusion Energi. As previously mentioned, this car was available for testing during this thesis. Table 3-5 provides the parameters for the radar and parking sensors. The maximum velocity for the parking sensors is calculated using the update frequency and assumed range. The maximum velocity for the radar is assumed to be 90 miles per hour, which converts to 144 kph.

Table 3-5: ADAS sensor properties

Sensor	Update Frequency [Hz]	Range [meters]	Cone Angle [Degrees]	Max Velocity Detected [kph]
Parking Sensor	5	5	30	90
Radar	20	60	30	144

To simulate ADAS data output for different scenarios, first a trajectory is created for the incoming object. The time for the trajectory is from 0 seconds to -2 seconds. The point of impact is 0 seconds; hence, -2 seconds is the ADAS data two seconds before the

impact. Once the trajectory is generated, for each update point for each sensor, it is checked to see if the object is within the sensor's range. If the object is in the sensor's range, then the output is generated. In table 3-1, it is defined that parking sensor data is unitless and radar data is in kph, so the simulated data output is the same.

3.6 Conclusion

The crash damage prediction system proposed in this chapter uses ADAS data while relying on simple parts of traditional damage prediction methods. While the system as shown in figure 3-1 cannot be tested as a whole, it can be tested by splitting it up. The crush prediction segment will be testing using NHTSA data. The location detection part will be tested using simulated ADAS data for different impact scenarios. In the system described in figure 3-1, crush and impact zones can be used to test the process to determine which parts are damaged. However, due to the different datasets used for crush prediction and location determination, the outputs of the two cannot be combined to test the process to determine which parts are damaged. Instead, the errors from each individual segment will be used to determine their effect, if any, on the damaged parts during an impact. The results of the tests of all three components of this method are shown in chapter 4.

CHAPTER 4. RESULTS AND DISCUSSION

In this chapter, the results obtained from methods in chapter 3 will be discussed. The following sections will begin with results for crush prediction and impact zone prediction. This will be followed by the effect of both aforementioned results on the final parts damaged determination.

4.1 Crush Prediction Results

4.1.1 Results

In this section, the results from the crush prediction analysis will be discussed. As discussed in section 3.5, the data used to test crush prediction is obtained from NHTSA crash tests. NHTSA crash tests are conducted for every new vehicle sold in the United States, however, only some of the tests are instrumented as required. To calculate crush, accelerometer data is needed from a crash test. NHTSA only instruments some side impact tests with accelerometers, specifically, impacts with a pole at 32 [kph] and impacts with a deformable barrier at 62 [kph].

Crush prediction was tested using crash pulse data from 76 different crash tests. Each of those tests was either an impact with a pole or an impact with a deformable barrier. Results for every single crash test are shown in the appendix A. Table 4-1 shows the average errors in predicting the crush value by vehicle type. It can be noted that the overall average error is -12.1%, meaning that for the 76 crash tests, crush was overestimated by 12.1%.

Table 4-1: Average crush error by vehicle type

Vehicle Type	Average Error [%]	Average Error (without cut-off point) [%]	Number of Vehicles
Compact	-8.3%	-233.0%	10
Coupe	9.2%	-92.5%	5
Sedan	-16.2%	-237.3%	16
SUV	-24.0%	-82.1%	21
Truck	-7.7%	-67.4%	21
Van	13.2%	-225.9%	3
Combined	-12.1%	-137.0%	76

Section 3.5 discusses challenges associated with using NHTSA data for crush prediction. One of the challenges is that the data ends inconsistently, meaning that the acceleration signal could end immediately after the impact or several seconds after the impact. If the signal does not end immediately after the impact, then that causes errors in the crush value. So, to reduce error, it was stated that a signal cut-off point was found for each test and used as the upper limit of integration for equation 5. The effect of using the cut-off point vs. end of the signal as the upper limit of integration can be seen in the results in table 4-1. The average error without using a cut-off point is -137%, and average error with the cut-off point is -12.1%, significantly lower. This reduction in error is seen across all vehicle types, with the largest reduction of 239% seen for minivans. The reduction in error is not referenced for crush results in the remainder of this chapter, however, if a test by test comparison is desired, it can be found in appendix A.

As mentioned earlier, data used for crush prediction is from two different types of impacts, poles and deformable barriers. Table 4-2 shows how the error differs for both impact types for each vehicle type and combined results. The combined average error for deformable barrier impacts is -10.7% and impacts with a pole is -14%. The total number

of vehicles tested was 76 with 43 of them being deformable barrier impacts and 33 being impacts with a pole.

Table 4-2: Average crush error by impact type

	Impact with a Deformable Barrier		Impact with a Pole	
Vehicle Type	**Average Error [%]**	**Number of Vehicles**	**Average Error [%]**	**Number of Vehicles**
Compact	5.1%	6	-28.5%	4
Coupe	12.0%	3	4.9%	2
Sedan	-16.8%	11	-15.0%	5
SUV	-35.9%	11	-10.8%	10
Truck	2.6%	10	-17.0%	11
Van	14.4%	2	10.7%	1
Combined	-10.7%	43	-14.0%	33

4.1.2 Discussion of Crush Results

From table 4-1, the average error for all vehicle types is -12.1%, however, more insight can be gained by breaking these results down further. SUVs have the largest absolute error of all vehicle types by -24%, more than three times the lowest absolute error of -7.7% for trucks. After SUVs, sedans have the largest absolute error, followed by vans, coupes, compacts, and trucks respectively. As section 4.3 will show, all of the errors shown will have minimal effect on the final determination of damaged parts. It should also be noted that on average, all of the vehicle types noted in table 4-1 overestimate the crush value, except for vans or coupes.

Assessing the results by impact type, the data shows a lower absolute error for impacts with deformable barriers than for impacts with poles. Impacts with deformable barriers are meant to represent an impact with a vehicle crash structure. For all vehicle types except sedans and SUVs, there is a lower error for impacts with poles than for

deformable barrier impacts. Deformable barrier impacts for sedans have an average error of -16.8% and impacts with pole for sedans have an average error of -15%, both of these are very close to each other. On the other hand, SUVs have a very large error of -35.9% for deformable barrier impacts and -10.8% for impacts with poles.

To gain a better understanding of the large error in deformable barrier impacts for SUVs, the 11 different tests are given below in table 4-3, arranged in descending order of absolute error. Note that all deformable barrier impacts are on the left side of a stationary vehicle at 62 [kph]. This information is also given in chapter 3 and appendix A. From table 4-3, the three largest errors are for NHTSA test numbers 10653, 10344, and 9486. The largest of these, test 10653, is not only the largest error for SUVs, but also the largest absolute error out of all 76 crash tests analysed. The effect these results have on the final determination of damaged parts is given in section 4.3.

Table 4-3: Crush results (deformable barrier impacts for SUVs)

NHTSA Test #	Year	Make	Model	Predicted Crush [cm]	Expected Crush (NHTSA) [cm]	Error [%]
10653	2019	Ford	Edge	41.7	19	-119.5%
10344	2018	Ford	Expedition	17	8.2	-107.3%
9486	2016	Ford	Explorer	43.2	23.8	-81.5%
10162	2018	Toyota	C-HR	26.2	15.8	-65.8%
10358	2018	Mazda	CX-5	16.7	12.2	-36.9%
9747	2017	Kia	Sportage	11.4	17.8	36.0%
9788	2016	Chevrolet	Tahoe	26.5	20.3	-30.5%
9786	2016	Nissan	Rogue	17.6	22	20.0%
10351	2018	Ford	EcoSport	15.1	12.7	-18.9%
9945	2017	GMC	Acadia	20.1	24	16.3%
10136	2018	Volkswagen	Atlas	21.3	19.9	-7.0%

Errors associated with SUVs can be analyzed in a different manner by splitting the vehicles by class. For SUVs, this would be either crossover, midsize, or large. The split results are given in table 4-4 where the average error for each type of SUV is also given with the number of vehicles in each class. This information can be used to determine if there is any specific class of SUV that has the largest error associated with it. From table 4-4, medium SUVs have a unibody design and have the largest absolute error. It is possible that medium SUVs have larger crush prediction error, however, this cannot be said for certain as there are only 3 medium SUVs. To definitively prove this, more medium SUVs would have to be tested with both a body on frame design and unibody design. However, this cannot be done due to a lack of data. So, for now, it cannot be said for certain that body on frame designs cause large crush prediction errors. Additionally, although large SUVs have the lowest absolute error, this relationship cannot be confirmed due to the same reason, low sample set.

Table 4-4: Crush errors by SUV class

Type of SUV	Average Error [%]	Body Type	Number of Vehicles
Crossover	-20.60%	Unibody	12
Midsize	-48.20%	Unibody	3
Large	-18.60%	Body on Frame	6
Combined	-24.00%		21

4.2 Impact Zone Prediction Results

In this section, the results from the impact zone prediction analysis will be discussed. As noted in section 3.5, analysis data for impact zone prediction was simulated for this specific purpose. The data in question is ACC radar and parking sensor data. As a recap, once the simulated data was obtained, it was analyzed using the algorithm described

in section 3.3. ADAS data was generated for 32 different impact scenarios, a majority of which were front and rear impacts. There were several side impact scenarios included, but due to a lack of sensor coverage, side impacts were not included in the same quantity as front and rear impacts. As a note, the algorithm used to analyze ADAS data outputs the impact zones on the vehicle, the impact zones are given in figure 3-7. Additionally, the parts located in each impact zone are given in table 3-2.

The results from the algorithm used to determine impact zones are given be below, but before discussing them, first the expected results must be introduced. Table 4-5 below gives the impact type, velocity, angle, and expected impact zone for each test. Note that test numbers here do not correspond to any published data, they are simply chosen for documentation purposes. From table 4-2, the range of velocities for front and rear impacts was from 10 [kph] to 90 [kph], and for side impacts in zone 22 it was 10 [kph] and 20 [kph]. For side impacts not in zone 22, the impact velocity is noted as not available due to it not being needed. All side impacts outside the range of parking sensors show the same sensor output, 0 for parking sensors (default value) and 255 [kph] for radar (default value) in ideal conditions and non-ideal conditions might have noise. It must be said that for this thesis, ADAS data was only generated for ideal conditions, although, chapter 5 does briefly cover a potential analysis method for non-ideal conditions. For ideal conditions, it is assumed that only sensors in the impact zone would have non-zero data.

Table 4-5: Impact zone prediction (test information and expected results)

Test #	Impact Type	Impact Side	Impact Area	Impact Velocity [kph]	Impact Angle	Expected Impact Zone
1	Full	Front	Full	90	0	[1 2 3 4 5]
2	Full	Front	Full	60	0	[1 2 3 4 5]
3	Full	Front	Full	30	0	[1 2 3 4 5]
4	Full	Front	Full	10	0	[1 2 3 4 5]
5	Full	Rear	Full	90	0	[12 13 14 15 16]
6	Full	Rear	Full	60	0	[12 13 14 15 16]
7	Full	Rear	Full	30	0	[12 13 14 15 16]
8	Full	Rear	Full	10	0	[12 13 14 15 16]
9	Pole	Front	Center	30	0	[3]
10	Pole	Front	Right	30	0	[2]
11	Pole	Front	Left	30	0	[4]
12	Pole	Front	Center	10	0	[3]
13	Pole	Front	Right	10	0	[2]
14	Pole	Front	Left	10	0	[4]
15	Pole	Front	Center	10	10	[3]
16	Pole	Front	Right	10	10	[2]
17	Pole	Front	Left	10	10	[4]
18	Pole	Side	Right-corner	10	20	[22]
19	Pole	Side	Right-corner	10	10	[22]
20	Pole	Rear	Center	10	0	[14]
21	Pole	Rear	Right	10	0	[15]
22	Pole	Rear	Left	10	0	[13]
23	Pole	Rear	Center	10	10	[14]
24	Pole	Rear	Right	10	10	[15]
25	Pole	Rear	Left	10	10	[13]
26	N/A	Side	N/A	N/A	0	[0]
27	Pole	Front	Center	15	10	[3]
28	Pole	Front	Right	15	10	[2]
29	Pole	Front	Left	15	10	[4]
30	Pole	Rear	Center	15	10	[14]
31	Pole	Rear	Right	15	10	[15]
32	Pole	Rear	Left	15	10	[13]

Table 4-5 gives the expected results for impact zone prediction, along with the impact information for each test. Table 4-6 gives the expected results along with the predicted results from the analysis. The table is color coded to make it easier to read, every row marked in yellow is a test where the expected results did not match the predicted results. For every other test, the expected results matched what was predicted using the algorithm, however, for the discussion section, a majority of the focus will be on the results that do not match and the cause of the errors.

Table 4-6: Impact zone prediction results

Test #	Impact Type	Impact Side	Impact Area	Predicted Impact Zone	Expected Impact Zone
1	Full	Front	Full	[3]	[1 2 3 4 5]
2	Full	Front	Full	[1 2 3 4 5]	[1 2 3 4 5]
3	Full	Front	Full	[1 2 3 4 5]	[1 2 3 4 5]
4	Full	Front	Full	[1 2 3 4 5]	[1 2 3 4 5]
5	Full	Rear	Full	N/A	[12 13 14 15 16]
6	Full	Rear	Full	[12 13 14 15 16]	[12 13 14 15 16]
7	Full	Rear	Full	[12 13 14 15 16]	[12 13 14 15 16]
8	Full	Rear	Full	[12 13 14 15 16]	[12 13 14 15 16]
9	Pole	Front	Center	[1 2 3 4 5]	[3]
10	Pole	Front	Right	[2]	[2]
11	Pole	Front	Left	[4]	[4]
12	Pole	Front	Center	[3]	[3]
13	Pole	Front	Right	[2]	[2]
14	Pole	Front	Left	[4]	[4]
15	Pole	Front	Center	[3]	[3]
16	Pole	Front	Right	[2]	[2]
17	Pole	Front	Left	[4]	[4]
18	Pole	Side	Right-corner	N/A	[22]
19	Pole	Side	Right-corner	[22]	[22]
20	Pole	Rear	Center	[14]	[14]
21	Pole	Rear	Right	[15]	[15]
22	Pole	Rear	Left	[13]	[13]

Table 4-6 continued

23	Pole	Rear	Center	[15]	[14]
24	Pole	Rear	Right	[15 16]	[15]
25	Pole	Rear	Left	[13]	[13]
26	N/A	Side	N/A	[0]	[0]
27	Pole	Front	Center	[3]	[3]
28	Pole	Front	Right	[2]	[2]
29	Pole	Front	Left	[4]	[4]
30	Pole	Rear	Center	[15]	[14]
31	Pole	Rear	Right	[15 16]	[15]
32	Pole	Rear	Left	[13]	[13]

4.2.1 Discussion of Impact Zone Results

From table 4-6, there are 8 tests where the predicted results did not match to the expected results. Each of those is for a specific reason, some of them are due to the sensor specifications and others due to sensor position. Starting from the beginning, test 1 is inaccurate due to the high impact velocity. From table 3-5, parking sensors have a maximum velocity of 90 [kph], calculated using the sensor update frequency and range. Further analysis showed that anything at 88 [kph] and above will not be visible on the parking sensor data. The reason it is 88 [kph] and not 90 [kph] is due to the parking sensor data being unitless, converting from distance to unitless numbers from 0 to 15 causes the 2 [kph] offset. The radar has max detection velocity of 144 [kph] or 90 [mph], which is why a full impact at 90 [kph] in test 1 was detected as an impact in zone 3. The same reasoning applies for test 5, but as the rear of the 2016 Ford Fusion Energi does not have a radar, that impact was not visible on parking sensor data.

For test 18, the impact is in zone 22, near the right-side parking sensors, at 20° from the center line. From table 3-5, parking sensors are assumed to have a cone angle of 30° or

15° from the center line. So, the angle for test 18 does not meet the sensor requirements, thus causing an error. Test 19 is a similar impact with a different impact angle and the predicted impact zone for test 19 is correct.

Tests 23 & 30 have the same type of error, there is an offset in the impact zone for a center impact in the rear at 10°. This error is simply because of the impact angle and the lack of a rear radar. The same impact type of impact at the front is predicted correctly due to radar data. Test 23 data can be visualized in figure 4-1, where the parking sensor data can be seen for 0.4 seconds before impact and 0.6 seconds before impact. The figure is just to provide an idea of what the data looks like for an angled impact. The error for tests 23 & 30 cannot be corrected due to the logic used, but as section 4.3 will show, this does not affect the final determination of damaged parts. The error for tests 24 & 31 occurs for the same reason as tests 23 & 30, due to the angle of impact and lack of rear radar. As with

tests 23 & 30, the final determination of damaged parts will not be affected by this offset in predicted results.

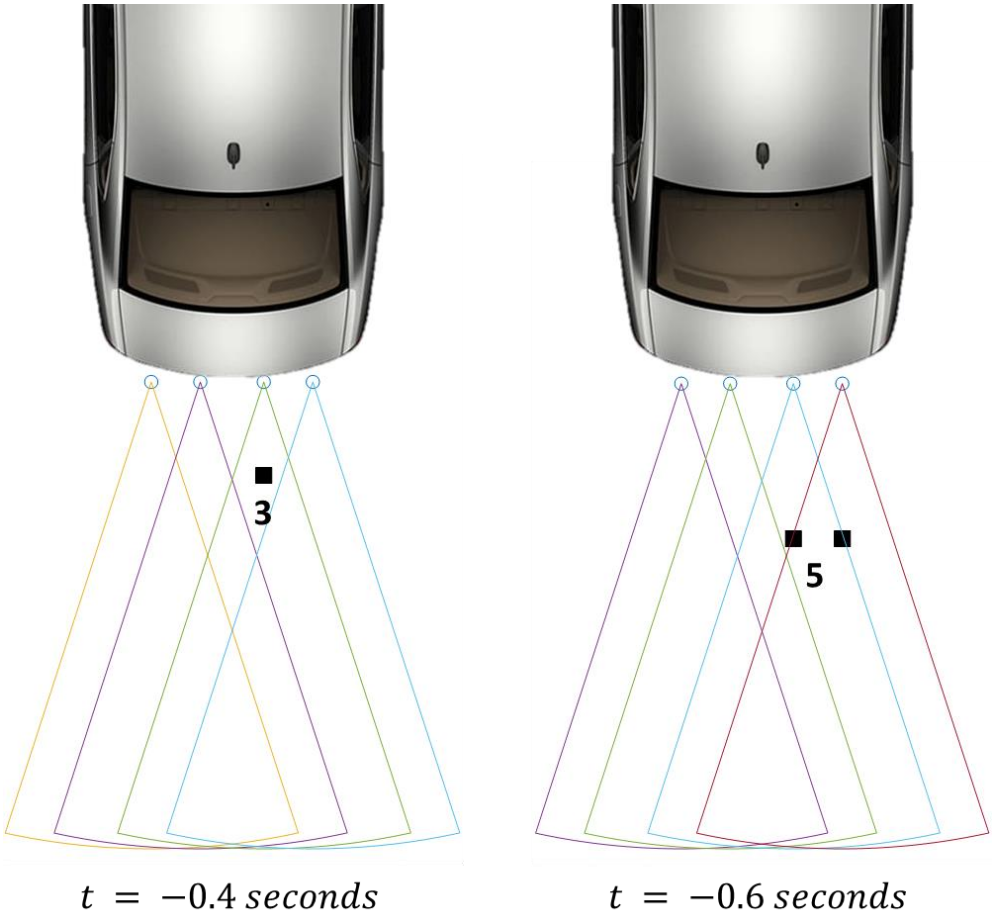

Figure 4-1: Simulated test 23

Finally, the last error to address is test 9, where a direct center impact at 30 [kph] is predicted as a full impact at 30 [kph]. This error is due to the sensor geometry on the 2016 Ford Fusion Energi and the assumed sensor specifications. From observing the simulated data and some investigation, it was determined that front center impacts with a pole above 25 [kph] look the same on parking sensor and radar data as full-frontal impacts above 25 [kph]. This effect is shown in figure 4-2, where left column is a front center

impact at 25 [kph] and right column is a front center impact at 26 [kph]. For a 25 [kph] impact, the last time the incoming object is seen on parking sensor data is 0.4 seconds before impact. However, if this were a full-frontal impact, the object would have been seen at 0.2 seconds before impact due to object being directly in front of the parking sensor. For a 26 [kph] front center impact, the last time the incoming object is seen on parking sensor data is 0.2 seconds before impact, the same as a full-frontal impact, thus the error. Unlike the previously discussed errors, this one will have an effect on the final determination of damaged parts due to the relatively large difference between the expected and predicted results.

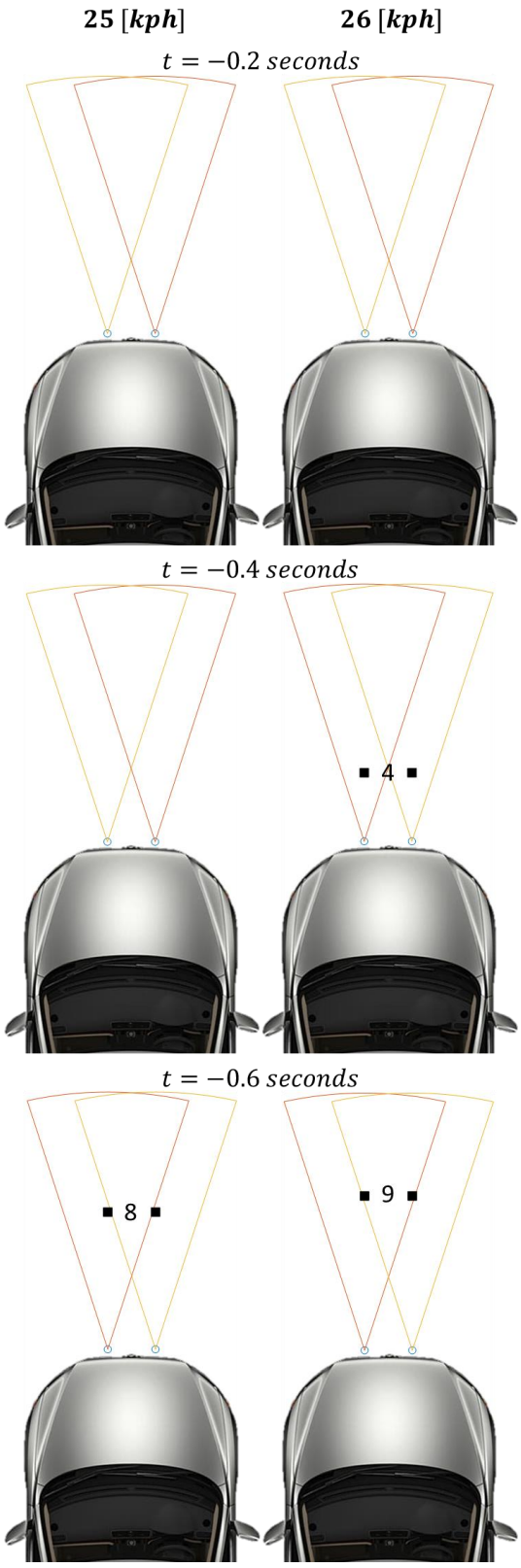

Figure 4-2: Front center impact comparison - 25 [kph] & 26 [kph]

4.3 Determining Parts Damaged

This section covers the effect of the results in sections 4.1 and 4.2 on the final determination of damaged parts. Before addressing those results, however, how they will be used will be discussed. The results in section 4.1 are for side impact NHTSA tests and the results in section 4.2 are for simulated impact scenarios. As the two never align, it is not appropriate to combine the results from the two sections to from a combination of crush and location. Due to this reason, a determination of damaged parts cannot be made for the results in the previous sections. However, what can be seen is the effect of the errors encountered in the crush and impact zone prediction results. So, this section will analyze the effect of the errors in the previous section. A worst case scenario will be analyzed where the errors have the largest effect and then the scenario tested in the relevant section will be analyzed. The end goal for every error is to show that it would not influence the final results. As it will be seen later, this holds true for most cases.

4.3.1 Effect of Crush Errors

To assess the worst possible effect of crush, the three largest absolute errors were analysed. Information regarding each of the tests associated with the largest absolute errors is given in table 4-7. Notice that the vehicles with the largest errors are all SUVs, which have the largest absolute average error for all vehicle types. Table 4-8 shows the effect on the final determination of damaged parts for each of the worst three vehicles.

Table 4-7: Vehicles with largest absolute crush error

NHTSA Test #	Year	Make	Model	Predicted Crush [cm]	Expected Crush (NHTSA) [cm]	Error [%]
10653	2019	Ford	Edge	41.7	19	-119.5%
10344	2018	Ford	Expedition	17	8.2	-107.3%
9486	2016	Ford	Explorer	43.2	23.8	-81.5%

From the data in table 4-8, tests 10653 & 9486 do not have a worst case scenario. This is due to their expected crush values being so large. From table 3-4, any crush value above 18 [cm] will affect the same parts. For the tests 10653 & 9486, the expected crush value is 19 [cm] and 23.8 [cm], respectively. So, for each of those, no matter what the impact zone is, there is maximum damage inflicted.

Test 10344 is different than the other two tests in table 4-8 due to the much lower expected crush value. For a crush of 8.2 [cm], the worst case scenario is a full-frontal impact. This can be confirmed by table 3-5, where a front impact with predicted crush of 17 [cm] would cause much more damage than the expected value of 8.2 [cm]. Due to the large error in the predicted crush value, the final determination shows fog lights, radiator, and hood being damaged in the worst case scenario. This is in addition to the parts that would be damaged, headlights and front bumper.

Looking at the testing scenario for each of the worst cases, the part damaged in all three impacts would be the door. The number of parts damaged does not increase even if the predicted crush value is used instead of the expected crush value. So, it can be said that for the tests conducted, the crush prediction error does not affect the final determination of damaged parts.

Finally, it is important to note that even though there are some test cases where the crush error is very large, as long as it does not affect the final outcome, the error is not important. The final outcome for this case is the determination of damaged parts. This is not to say that the error is not important, but as long as it does not affect the final outcome, it is deemed acceptable. The reason for this goes back to the original goal of this thesis, which was to make one of three determinations for a given impact. The first one being if the car is drivable with light damage, the second one being if the car is repairable with extensive damage, and the last one being if the car is totaled. For each of those, if that determination can be made, even with some error in crush measurements, that error is deemed acceptable.

Table 4-8: Effect of largest crush errors on determination of damaged parts

NHTSA Test #	Predicted Crush [cm]	Expected Crush (NHTSA) [cm]	Worst Case Impact Zone(s)	Expected Impact Zone	Parts Damaged (Worst Case)	Parts Damaged Due to Error (Worst Case)	Parts Damaged (Actual Impact Zone)
10653	41.7	19	N/A	[8 9]	N/A	N/A	Doors
10344	17	8.2	[1 2 3 4 5]	[8 9]	Headlights and Bumper	Fog lights, radiator, and hood	Doors
9486	43.2	23.8	N/A	[8 9]	N/A	N/A	Doors

4.3.2 Effect of Impact Zone Errors

To assess the effect of the impact zone prediction errors, the scenarios discussed in section 4.2.1 are used. Each of the scenarios discussed in that section is given in table 4-9 along with the effect those errors have on the final determination of damaged parts. From the 8 error scenarios, tests 1 & 5 have the largest effect on the final determination. For test 1, due to the underestimation of the impact zone, headlights, fog lights, and parts of the

bumper are missed in the assessment. For test 5, all rear components are missed in the assessment due to the high-speed impact scenario where no impact zones were predicted. Test 18 has a similar effect on the final assessment as tests 1 & 5, the front right fender and bumper are missed due to the impact angle being too large.

Test 9 is different than most other tests due to the overestimation of the impact zones. Instead of a front center impact, a full-frontal impact is predicted. This causes a large overestimation of the damaged parts. Instead of just the bumper, hood, and radiator being damaged for the expected results in test 9, the predicted results cause the headlights, fog lights, and sides of the bumper to be damaged.

Tests 23, 24, 30, and 31 are much different than the previous four discussed, where there was a discrepancy in the damaged parts between the predicted and expected impact zones. For tests 23, 24, 30, and 31, there was no difference in the damaged parts for the predicted and expected impact zones. From table 3-4, this is due to the same grouping of parts being in the areas impacted. The number of parts damaged increases for certain scenarios, and for each of those scenarios, the error was caused due to impact scenarios exceeding sensor specifications.

Table 4-9: Effect of impact zone prediction errors on determination of damaged parts

Test #	Impact Type	Impact Side	Impact Zone	Predicted Impact Zone	Expected Impact Zone	Parts Missed
1	Full	Front	Full	[3]	[1 2 3 4 5]	Headlights, fog lights, and parts of the bumper
5	Full	Rear	Full	[0]	[12 13 14 15 16]	All rear components
9	Pole	Front	Center	[1 2 3 4 5]	[3]	No parts missed, but overestimates damage

Table 4-9 continued

18	Pole	Front	Corner	[0]	[22]	Front right side fender and bumper
23	Pole	Rear	Center	[15]	[14]	N/A
24	Pole	Rear	Right	[15 16]	[15]	N/A
30	Pole	Rear	Center	[15]	[14]	N/A
31	Pole	Rear	Right	[15 16]	[15]	N/A

4.4 Conclusion

In this chapter, the results obtained using the methods in chapter 3 were discussed. From chapter 3, the methods were split into three sections, crush prediction, impact zone prediction, and determining the damaged parts. This chapter provided results for crush and impact zone prediction and analyzed the effect of the corresponding errors on the determination of damaged parts. Crush prediction analysis showed gave an average error of -12.1%. Breaking that down by vehicle type, SUVs had the highest absolute error at -24% and trucks had the lowest at 7.7%. From there, ADAS data was analyzed for impact zone prediction. The results showed that impacts outside the parking sensor and radar specification always caused an error. An example of this is an impact velocity higher than the maximum sensor detection velocity. Finally, the errors from the two previous results were analyzed for their effect on the determination of the parts damaged. This showed that crush prediction error had a minimal effect on the parts damaged when the crush was above 18 [cm]. Impact zone error had a larger effect on the parts damaged due to certain impact zones having different parts than others. It can be concluded, however, that for low velocity front and rear impacts, the impact zone errors should have minimal effect on the determination of damaged parts.

CHAPTER 5. SUMMARY AND FUTURE WORK

5.1 Summary

The goal of this thesis was to use ADAS data to predict which parts are damaged on a vehicle after impact. A system, as shown in chapter 3, was designed to do so using a combination of crash pulse analysis and ADAS data. The system was divided up into three main components, obtaining crush, impact zone, and predicting which parts are damaged on the vehicle. To prove this system, accelerometer data was obtained from NHTSA crash tests was used for crush prediction and simulated ADAS data was used for impact zone prediction. Theoretically, the two would then be combined to determine which parts are damaged on the vehicle. However, for the purposes of this thesis, their errors were analyzed for their effect on determining damaged parts. The crush prediction results shown in section 4.1 show an average error of -12.1%. It was also shown that SUVs have the largest absolute error and trucks have the lowest. From there, section 4.2 showed the results for impact zone prediction. As discussed previously, impact zone prediction results were acquired using simulated data. The impact zone prediction errors were associated with impact scenarios outside the assumed sensor specification. The effect of the errors in section 4.1 and 4.2 are shown in section 4.3. It was shown that, even for worst case scenarios, the largest absolute crush errors had no effect on the final determination of damaged parts if the expected crush values were larger than 18 [cm]. Impact zone errors did have an effect on the final determination of damaged parts; however, the effect was limited to impact scenarios outside the assumed sensor specifications. Overall, NHTSA data proved the crush prediction part and the simulated data proved the impact zone prediction part. The errors

resulting from both were used to assess the feasibility of determining damaged parts. It can be concluded that crush and impact zone location, even with error, can be used to determine which parts are damaged on the vehicle.

5.2 Future Work

For the damage prediction system to be implemented, more development needs to be done on the individual parts discussed in this thesis. From the results in this thesis, crush prediction error is shown to be -12.1%, however, this is for side impacts. Although there are examples in the literature discussed in chapter 2 using the crush prediction method discussed in this paper for front and rear impacts, further testing using additional crash test data is warranted. Additionally, the ADAS data used for impact zone prediction was simulated, so some experimental data would be required for additional testing. This is a challenge for anyone using publicly available data as most crash testing authorities do not instrument front and rear impacts with accelerometers or provide any ADAS data for crash tests.

Impact zone prediction is done using logic developed for sensors on a 2016 Ford Fusion Energi, however, there are other methods that can be used for impact zone prediction. A convolution neural network could be used to determine impact zones; however, it would have to be trained properly, using a large dataset. Although this would cause additionally work, a properly trained neural network would be versatile. Once a neural network structure is established, updated weights could be fed to it as a better training is achieved.

APPENDIX A. CRUSH PREDICTION RESULTS

Crush prediction values for every crash test analyzed are shown here in appendix A. There are results showing crush obtained with and without a cut-off point, and their corresponding errors. Additionally, each test's NHTSA test number is given and the corresponding vehicle models. For each model, the body type and vehicle type are given. Vehicle type is the type of car it is, for example, a sedan or sports utility vehicle (SUV). Body type is one of two things, either a unibody design or a body on frame design. The impact side is also given, but it must be noted that all impacts are left side impacts. Vehicle velocity and impact velocity are given, note that they are not the same thing. It is possible for the vehicle velocity to be 0, but the impact velocity to be 62 [kph].

To make the table fit better on this page layout, it is split into two tables, A-1 and A-2.

Table A-1: Crush results (vehicle and impact information)

NHTSA Test #	Year	Make	Model	Vehicle Type	Body Type	Impact Type	Impact Side
9983	2017	Toyota	Yaris	Compact	Unibody	Deformable Barrier	Left
10356	2018	Nissan	Rogue	SUV	Unibody	Pole	Left
10166	2018	Hyundai	Sante Fe	SUV	Unibody	Pole	Left
10192	2018	Honda	Accord 1.5T LX	Sedan	Unibody	Pole	Left
10194	2018	Mercedes-Benz	GLC300	SUV	Unibody	Pole	Left
10358	2018	Mazda	CX-5	SUV	Unibody	Deformable Barrier	Left
10569	2019	Nissan	Frontier	Truck	Unibody	Pole	Left
9968	2017	Chevrolet	Camaro	Coupe	Unibody	Deformable Barrier	Left

Table A-1 continued

9986	2017	Toyota	Corolla	Sedan	Unibody	Deformable Barrier	Left
9990	2017	Buick	LaCrosse	Sedan	Unibody	Deformable Barrier	Left
9995	2017	Audi	A4	Sedan	Unibody	Deformable Barrier	Left
9996	2017	Mercedes-Benz	E-Class	Sedan	Unibody	Deformable Barrier	Left
10003	2017	Chevrolet	Volt	Sedan	Unibody	Deformable Barrier	Left
10032	2017	Honda	Ridgeline	Truck	Unibody	Deformable Barrier	Left
10035	2017	Nissan	Titan	Truck	Unibody	Deformable Barrier	Left
10038	2017	Smart	Fortwo	Compact	Unibody	Deformable Barrier	Left
10046	2017	Lexus	IS 200t	Sedan	Unibody	Deformable Barrier	Left
10162	2018	Toyota	C-HR	SUV	Unibody	Deformable Barrier	Left
10054	2016	Toyota	Prius	Sedan	Unibody	Deformable Barrier	Left
10132	2018	Honda	Odyssey	Van	Unibody	Deformable Barrier	Left
10136	2018	Volkswagen	Atlas	SUV	Unibody	Deformable Barrier	Left
9746	2017	Kia	Sportage	SUV	Unibody	Pole	Left
9747	2017	Kia	Sportage	SUV	Unibody	Deformable Barrier	Left
9756	2016	Nissan	Versa	Compact	Unibody	Deformable Barrier	Left
9779	2016	Chevrolet	Cruze	Sedan	Unibody	Pole	Left
9780	2016	Nissan	Rogue	SUV	Unibody	Pole	Left
9781	2016	Chevrolet	Tahoe	SUV	Body on Frame	Pole	Left
9782	2016	Chevrolet	Malibu	Sedan	Unibody	Pole	Left
9783	2016	Honda	Fit	Compact	Unibody	Pole	Left
9785	2015	Toyota	Sienna	Van	Unibody	Pole	Left
9786	2016	Nissan	Rogue	SUV	Unibody	Deformable Barrier	Left
9788	2016	Chevrolet	Tahoe	SUV	Body on Frame	Deformable Barrier	Left

Table A-1 continued

9790	2015	Toyota	Sienna	Van	Unibody	Deformable Barrier	Left
9792	2017	Hyundai	Elantra	Sedan	Unibody	Pole	Left
9794	2017	Hyundai	Elantra	Sedan	Unibody	Deformable Barrier	Left
9803	2016	Buick	Cascada	Coupe	Unibody	Pole	Left
9809	2016	Honda	Civic	Sedan	Unibody	Pole	Left
9810	2016	Honda	Civic	Sedan	Unibody	Deformable Barrier	Left
9819	2016	Buick	Cascada	Coupe	Unibody	Deformable Barrier	Left
9940	2016	Chevrolet	Cruze	Sedan	Unibody	Deformable Barrier	Left
9941	2017	Mitsubishi	Mirage	Compact	Unibody	Pole	Left
9942	2017	Mitsubishi	Mirage	Compact	Unibody	Deformable Barrier	Left
9945	2017	GMC	Acadia	SUV	Unibody	Deformable Barrier	Left
9947	2017	GMC	Acadia	SUV	Unibody	Pole	Left
10792	2019	Ford	F-250	Truck	Unibody	Deformable Barrier	Left
10791	2019	Ford	F-250	Truck	Unibody	Pole	Left
10777	2019	Ford	F-250	Truck	Unibody	Pole	Left
10774	2019	Ford	F-250	Truck	Unibody	Deformable Barrier	Left
10718	2019	Ford	F-250	Truck	Unibody	Deformable Barrier	Left
10715	2019	Ford	F-250	Truck	Unibody	Pole	Left
10653	2019	Ford	Edge	SUV	Unibody	Deformable Barrier	Left
10649	2019	Ford	Edge	SUV	Unibody	Pole	Left
10355	2018	Ford	Fiesta	Compact	Unibody	Deformable Barrier	Left
10354	2018	Ford	Fiesta	Compact	Unibody	Pole	Left
10352	2018	Ford	EcoSport	SUV	Unibody	Pole	Left
10351	2018	Ford	EcoSport	SUV	Unibody	Deformable Barrier	Left
10344	2018	Ford	Expedition	SUV	Body on Frame	Deformable Barrier	Left
10184	2018	Ford	Mustang	Coupe	Unibody	Pole	Left
10186	2018	Ford	Mustang	Coupe	Unibody	Deformable Barrier	Left

Table A-1 continued

10172	2018	Ford	F-150 SuperCrew	Truck	Unibody	Deformable Barrier	Left
10171	2018	Ford	F-150 SuperCrew	Truck	Unibody	Pole	Left
10164	2018	Ford	F-150 SuperCrew	Truck	Unibody	Deformable Barrier	Left
10163	2018	Ford	F-150 SuperCrew	Truck	Unibody	Pole	Left
10067	2017	Ford	Focus RS	Compact	Unibody	Pole	Left
10066	2017	Ford	Focus RS	Compact	Unibody	Deformable Barrier	Left
10006	2017	Ford	F-250 SuperCab	Truck	Unibody	Pole	Left
9998	2017	Ford	F-250 CrewCab	Truck	Unibody	Deformable Barrier	Left
9979	2017	Ford	F-250 CrewCab	Truck	Unibody	Pole	Left
9784	2016	Ford	F-150	Truck	Unibody	Pole	Left
9777	2017	Ford	Fusion	Sedan	Unibody	Deformable Barrier	Left
9545	2016	Ford	F-250	Truck	Unibody	Deformable Barrier	Left
9486	2016	Ford	Explorer	SUV	Unibody	Deformable Barrier	Left
9485	2016	Ford	Explorer	SUV	Unibody	Pole	Left
9474	2016	Ford	F-250 SuperCab	Truck	Unibody	Deformable Barrier	Left
9473	2016	Ford	F-250	Truck	Unibody	Pole	Left
9469	2016	Ford	F-250	Truck	Unibody	Pole	Left

Table A-2: Crush results (impact velocity, vehicle velocity, and error)

NHTSA Test #	**Rounded Velocity [kph]**	**Vehicle Velocity [kph]**	**Predicted Crush (without cut-off point) [cm]**	**Predicted Crush [cm]**	**Expected Crush (NHTSA) [cm]**	**Error (without cut-off point) [%]**	**Error [%]**
9983	62	0	12.5	11.8	14	10.7%	15.7%
10356	32	32	41.7	40.2	42	0.7%	4.3%
10166	32	32	40.2	40.2	37.7	-6.6%	-6.6%
10192	32	32	52.5	44.7	33.7	-55.8%	-32.6%

Table A-2 continued

10194	33	33	38.4	38.4	31.8	-20.8%	-20.8%
10358	62	0	19.7	16.7	12.2	-61.5%	-36.9%
10569	32	32	45.7	44.2	47.8	4.4%	7.5%
9968	62	0	9.5	7	16	40.6%	56.3%
9986	62	0	133.8	19.7	20.5	-552.7%	3.9%
9990	62	0	52.2	44	33.2	-57.2%	-32.5%
9995	62	0	148.3	27	21.7	-583.4%	-24.4%
9996	62	0	125.4	24.9	15.4	-714.3%	-61.7%
10003	62	0	44.8	25.9	23	-94.8%	-12.6%
10032	62	0	38	25.1	23.1	-64.5%	-8.7%
10035	62	0	24.9	24.4	24.1	-3.3%	-1.2%
10038	62	0	67.1	9.3	9.6	-599.0%	3.1%
10046	62	0	129.4	22.8	20.2	-540.6%	-12.9%
10162	62	0	56.6	26.2	15.8	-258.2%	-65.8%
10054	62	0	67	25.4	19.3	-247.2%	-31.6%
10132	62	0	148.4	20.2	19.8	-649.5%	-2.0%
10136	62	0	126	21.3	19.9	-533.2%	-7.0%
9746	32	32	39	28.1	32.4	-20.4%	13.3%
9747	62	0	37.9	11.4	17.8	-112.9%	36.0%
9756	62	0	263.1	29.9	24.6	-969.5%	-21.5%
9779	32	32	45.2	38.3	32	-41.3%	-19.7%
9780	32	32	58.4	54.3	39	-49.7%	-39.2%
9781	32	32	60	42.7	40	-50.0%	-6.8%
9782	32	32	34.8	30.5	34.5	-0.9%	11.6%
9783	32	32	37.2	35.6	27.4	-35.8%	-29.9%
9785	32	32	30.8	30.8	34.5	10.7%	10.7%
9786	61	0	17.9	17.6	22	18.6%	20.0%
9788	62	0	26.5	26.5	20.3	-30.5%	-30.5%
9790	62	0	31.1	15.5	22.4	-38.8%	30.8%
9792	32	32	42	40.9	28	-50.0%	-46.1%
9794	62	0	71.5	22.4	19.7	-262.9%	-13.7%
9803	32	32	52.8	24.9	26	-103.1%	4.2%
9809	32	32	30.4	24.7	28	-8.6%	11.8%
9810	61	0	15	18.2	15.8	5.1%	-15.2%
9819	62	0	26.7	19.14	14.4	-85.4%	-32.9%
9940	62	0	19.8	19.6	22.4	11.6%	12.5%
9941	32	32	43.1	39.8	32.7	-31.8%	-21.7%
9942	62	0	23	26.5	24	4.2%	-10.4%

Table A-2 continued

9945	62	0	19.6	20.1	24	18.3%	16.3%
9947	32	32	43.4	35.1	34.2	-26.9%	-2.6%
10792	62	0	6.7	6.7	14.4	53.5%	53.5%
10791	32	32	50.4	50.4	38.3	-31.6%	-31.6%
10777	32	32	43.8	43.8	34.8	-25.9%	-25.9%
10774	62	0	36.4	17.9	22.8	-59.6%	21.5%
10718	62	0	41.5	23	19.1	-117.3%	-20.4%
10715	32	32	47.1	43.1	28.3	-66.4%	-52.3%
10653	62	0	66.1	41.7	19	-247.9%	-119.5%
10649	32	32	44.6	44.1	39.2	-13.8%	-12.5%
10355	62	0	54.9	13.5	21.9	-150.7%	38.4%
10354	33	33	38.6	34.5	29.3	-31.7%	-17.7%
10352	33	33	38.5	37.7	31.2	-23.4%	-20.8%
10351	62	0	19.1	15.1	12.7	-50.4%	-18.9%
10344	62	0	18.2	17	8.2	-122.0%	-107.3%
10184	32	32	47.8	32.2	34.1	-40.2%	5.6%
10186	62	0	62.2	14.5	16.6	-274.7%	12.7%
10172	62	0	31.8	20.1	24.5	-29.8%	18.0%
10171	32	32	47.5	47.5	38.4	-23.7%	-23.7%
10164	62	0	121.4	38.5	25.2	-381.7%	-52.8%
10163	32	32	46.9	44.8	38.7	-21.2%	-15.8%
10067	32	32	58.1	57.6	39.8	-46.0%	-44.7%
10066	62	0	133.6	21.7	23	-480.9%	5.7%
10006	32	32	67.4	48	46.5	-44.9%	-3.2%
9998	62	0	36.9	10.8	20.1	-83.6%	46.3%
9979	32	32	49.3	48.7	32.6	-51.2%	-49.4%
9784	32	32	34.3	30.8	39.4	12.9%	21.8%
9777	62	0	172.6	23.6	24.5	-604.5%	3.7%
9545	62	0	103.7	34.1	28.8	-260.1%	-18.4%
9486	62	0	51.6	43.2	23.8	-116.8%	-81.5%
9485	33	32	49.6	48.9	42.1	-17.8%	-16.2%
9474	62	0	91.7	35.2	31.4	-192.0%	-12.1%
9473	32	32	85.7	77.8	68.3	-25.5%	-13.9%
9469	32	32	62.6	60.5	60.3	-3.8%	-0.3%

CHAPTER 6. REFERENCES

Connor JT, M. R., and Atlas LE (1994). Recurrent neural networks and robust time series prediction. *IEEE Trans Neural Netw, 5*(2), 240-254.

Huang, M. (2002). *Vehicle Crash Mechanics* CRC Press.

Karel A. Brookhuis, D. d. W. a. W. H. J. (2001). Behavioural impacts of Advanced Driver Assistance Systems–an overview. *European Journal of Transportation and Infrastructure Research, 1*(3), 245-253.

Kristofer D. Kusano, H. C. G. (2012). Automated crash notification: Evaluation of in-vehicle principal direction of force estimations. *Transportation Research Part C: Emerging Technologies, 32*, 116-128.

Muraspahic, D. Y. M. a. S. (2013). *Signal Analysis, Modeling and Simulation of Vehicle Crash Dynamics.* (Master's of Science), University of Agder, Kristiansand, Norway.

Paul Baguley, Rajkumar Roy, and James Watson. (2009). UNDERSTANDING THE COST OF DESIGN EVALUATION USING VIRTUAL CRASH TESTING. In *Research into Design: Supporting Multiple Facets Of Product Development* (pp. 176-182).

Pawlus, W. (2011). Mathematical modeling and parameters estimation of a car crash using data-based regressive model approach. *Applied Mathematical Modeling, 35*(5091-5107).

Vipin Kumar Kukkala, J. T., Sudeep Pasricha, and Thomas Bradley. (2018). Advanced Driver-Assistance Systems. *IEEE Consumer Electronics Magazine, 7*, 18-25.

Witold Pawlus, H. R. K., and Kjell G. Robbersmyr. (2013). Investigation of vehicle crash modeling techniques: theory and application. *International Journal of Advanced Manufacturing Technology, 70*, 965-996.

Witold Pawlus, H. R. K., Kjell G. Robbersmyr. (2010). Development of lumped-parameter mathematical models for a vehicle localized impact. *Journal of Mechanical Science and Technology, 25*(7), 1737-1747. doi:DOI 10.1007/s12206-011-0505-x